



Impact of Vertical Vibration on Group Piles During Earthquake Loading: Experimental Findings

Bilal J. Noman^{1*}, Bushra S. Albusoda¹

¹ Department of Civil Engineering, College of Engineering, University of Baghdad, Baghdad, Iraq.

Received 04 May 2024; Revised 14 September 2024; Accepted 21 September 2024; Published 08 October 2024

Abstract

This study presents novel research on the impact of vertical vibration on the dynamic response of pile groups embedded in stratified soil under seismic loading conditions. An experimental setup was employed wherein the piled machine foundation was subjected to vertical vibrations at three operating frequencies (10, 20, and 30 Hz) and subsequently exposed to four levels of seismic acceleration (0.1 g, 0.34 g, 0.77 g, and 0.82 g). Piles with a length-to-diameter ratio of 25 were embedded in a stratified soil profile, with an upper loose layer (30% relative density) and a lower dense layer (80% relative density) acting as end-bearing. Measurements and analyses of horizontal and vertical accelerations, and amplification factors were conducted using the Fast Fourier Transform (FFT), spectral acceleration (Sa), and variation of acceleration with depth. The results demonstrated a significant reduction in horizontal acceleration, with a peak ground acceleration (PGA) reduction of up to 64% in average, particularly at higher frequencies such as 30 Hz. The mitigation efficiency at 30Hz improved with increasing PGA, showing reductions of 42, 68, 75, and 63% for seismic accelerations of 0.1 g, 0.34 g, 0.77 g, and 0.82 g, respectively. The analysis further revealed harmonic resonance and higher mode effects at lower frequencies, with nonlinear soil behavior affecting the resonance and amplification patterns. Additionally, the results demonstrate that the far-field accelerations exceeded the near-field accelerations within the pile group, particularly in the surface layer. The results indicated that the initial vibration amplitudes exceeded the safe operating limits outlined in ACI 351.3R-18 under seismic loading, particularly at higher seismic acceleration levels and lower frequencies. Additional modified charts were presented to account for these conditions. The results presented promising evidence for using vertical vibrations as an earthquake-mitigation strategy. However, avoiding operating at frequencies less than 10 Hz is recommended because of the potential resonance and interaction with horizontal accelerations during earthquakes.

Keywords: Seismic Mitigation; Vertical Vibration; Machine Vibration Charts; Pile Foundations; Spectral Acceleration (SA); Fast Fourier Transform (FFT).

1. Introduction

Pile foundations are extensively employed in weak soil deposits to support various structures. Pile foundations are frequently exposed to dynamic loads generated by machinery-induced vibrations, ocean waves, seismic events, and static loads. As infrastructure projects continue to grow in scale and complexity, including offshore platforms, skyscrapers, nuclear power facilities, electric power stations, and other applications, there has been an increased emphasis on understanding the dynamic behavior of pile foundations. Despite numerous theoretical models and experimental investigations of pile-soil-pile systems, a significant gap exists in understanding the combined effects of vertical vibrations and seismic loading on pile foundations.

* Corresponding author: bilal.noman2001d@coeng.uobaghdad.edu.iq

 <http://dx.doi.org/10.28991/CEJ-SP2024-010-010>



© 2024 by the authors. Licensee C.E.J, Tehran, Iran. This article is an open access article distributed under the terms and conditions of the Creative Commons Attribution (CC-BY) license (<http://creativecommons.org/licenses/by/4.0/>).

Numerous analytical and semi-analytical methodologies have been proposed to investigate pile dynamic response, with Novak's continuum approach [1] gaining widespread practical adoption. This approach incorporates radiation damping and provides valuable insights into pile behavior under dynamic loading conditions. Novak [2] and Novak & Sharnouby [3] employed similar models to establish impedance functions for all vibration modes. Novak & Aboul-Ella [4, 5] further extended this approach to accommodate layered soil profiles with varying soil and pile properties across different layers. To account for nonlinear response, Novak [6] introduced the boundary zone concept, a simplified method for integrating modified properties into linear theory for practical applications. Additionally, several studies [7-9] employed continuum approach analysis to determine the dynamic response of soil-pile systems, considering soil nonlinearity, slippage, and separation at the system interface to establish pile responses under various vibration modes. Chau & Yang [10] extended the continuum approach to three-dimensional pile foundation analysis, incorporating soil nonlinearity into the modeling process.

The finite element (FE) method has gained significant prominence in addressing dynamic soil-pile-structure interaction challenges. Krishnan et al. [11] and Wu & Finn [12] have conducted FE analyses to investigate the dynamic response of single piles and pile groups. Kaynia [13] as well as Banerjee et al. [14] presented rigorous boundary element formulations to evaluate pile foundation dynamic response. Ayothiraman & Boominathan [15] employed the FE software PLAXIS to predict pile response to dynamic lateral loads. Finite element analysis has been employed to investigate the behavior of vertically vibrating machines in sand [16-18] to study the behavior of vertical vibrations induced by machines in sand and closed-end pipe piles under seismic loads [19-21]. Experimental studies have also explored the dynamic response of single piles embedded in dry and saturated sandy soil subjected to opposing rotary machine excitation using small-scale physical models [22-24]. Choudhary et al. [25] conducted an experimental and analytical investigation on the dynamic coupled response of 6-pile groups with different patterns.

The efficacy of analytical models has been validated through experimental test results, with dynamic forced vibration tests on piles categorized as either full-scale or small-scale. Due to their lower cost, shorter duration, and greater control over field conditions, small-scale tests are generally favoured for understanding pile dynamic response. Khandelwa et al. [26] investigated the behavior of short piles under lateral vibration, while Biswas and Manna [27] conducted model tests on single and group piles to determine soil-pile separation length during lateral vibration. Bhowmik et al. [28] and Bhowmik et al. [29] performed model tests on hollow steel piles under lateral and vertical harmonic loading. Bharathi et al. [30] studied the dynamic response of batter piles subjected to vertical vibration. The recent evolution of structures has expanded research to include pile groups. Choudhary et al. [31] conducted experimental tests to understand the impact of soil-pile interaction on different pile group configurations under coupled vibration, while Choudhary et al. [32] investigated the influence of pile arrangements on the dynamic response of pile groups. Additionally, recent full-scale tests by Sudhi et al. [33] have investigated the dynamic performance of floating piles under coupled vibrations. The studies extended in this area are scant due to its complexity in analysis.

Building on the insights gained from vertical vibration studies, it is imperative to address the behavior of pile foundations under seismic loading. The combined influence of vertical vibrations and earthquakes presents unique challenges and has been less thoroughly examined. Observations from major earthquakes (e.g., Mexico City 1985, Kobe 1995, Chi-Chi 1999, Bhuj 2001, Niigata 2004) [34] and Kahramanmaras 2023 [35] have revealed significant settlement and tilting in pile-supported structures on loose to dense sands or layered soils. Damage often occurs at pile interfaces or soil-layer boundaries. Modern theories recognize the influence of both inertial effects from superstructures and kinematic effects from surrounding soils on pile seismic behavior. Analytical studies using Winkler foundation models have explored soil nonlinearity and stiffness degradation [36-39].

Expanding on the knowledge gained from studying seismic loading, it becomes crucial to address the combined effects of vertical vibrations and earthquakes on pile foundations. Although substantial research has been devoted to seismic effects, the interaction between vertical vibrations and seismic loading remains underexplored. Liu [40] provides a contribution by examining the foundation design of large dynamic equipment in high-seismic areas. Through finite element modeling and modal analysis, Liu's study addresses dynamic and seismic loads on foundation-supporting equipment such as combustion turbine generators (CTG) and steam turbine generators (STG). The key seismic risks identified included ground shaking, liquefaction, and differential settlement, highlighting the necessity of deep foundations for mitigating these risks. Liu's findings align with recommendations in ACI 351-3R (2018), which suggest reducing the load ratio by a factor of 2.5 for block foundations with piles or springs. Arya et al. [41] suggested that the pile cap mass should be 1.5 to 2.5 times that of centrifugal machines and 2.5 to 4 times for reciprocating machines.

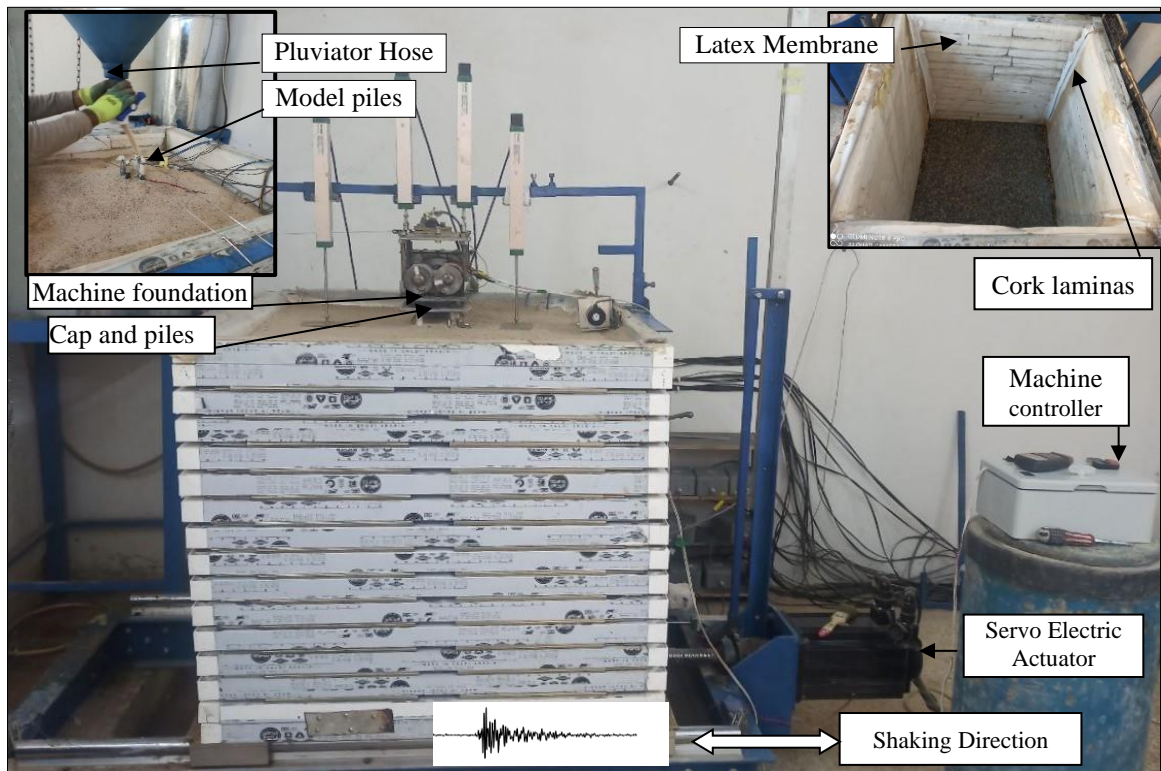
Tripathy & Desa [42] further analyzed the impact of seismically induced vibrations on turbomachinery foundations across various soil conditions using SAP 2000 software. They applied earthquake loading in northeast and southwest directions. They concluded that barrettes with rafts are optimal for high-seismic areas across all soil conditions, as they effectively transfer seismic reactions through columns to barrettes, thereby enhancing stability and durability. During strong-motion earthquakes, the turbomachinery foundation operating at a frequency of 65 Hz often vibrates out of phase owing to differing dynamic characteristics, leading to relative displacement if the top deck lacks sufficient capacity to handle the dynamic motions of machinery parts. Under poor soil conditions, such as those classified as NEHRP D, the foundation experiences increased displacement, bending moment, and base shear. The study recommends using geosynthetics with barrettes to minimize the displacement at the top deck under such conditions. Noman & Albusoda [43, 44] reviewed experimental studies and numerical models for machine foundations under seismic loads and concluded that the soil-structure interaction (SSI) can either enhance performance by reducing dynamic stiffness or cause failure owing to nonlinear soil behavior.

Despite extensive studies and significant efforts in this field, critical questions remain: What happens when vertical vibration is combined with seismic loading? Are the behaviors observed under each dynamic load individually consistent when both are applied together? Current research that addresses this complex and realistic scenario in theory and practice is limited. This study presents an innovative experimental investigation into the combined effects of vertical vibrations and seismic loading on mass pile foundations, aiming to bridge this significant gap in understanding.

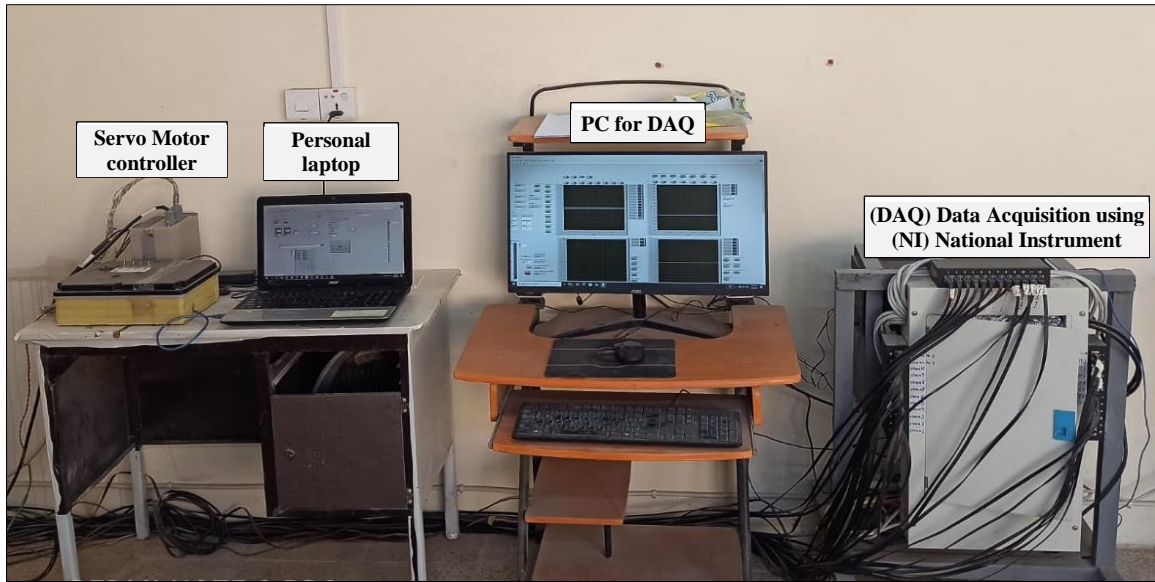
2. Experimental Setup and Testing

2.1. Shaking Table Test

The shaking table used in the experiments resulted from the collaborative efforts between the author and the College of Engineering at the University of Diyala. The devices were manufactured according to technical specifications and calibrated under the supervision of the author. The shake table, as shown in Figure 1, is attached to a servo motor with a maximum acceleration of 1.8 g under a 10kN payload and 2 g when running empty and has an input wave frequency range of 0.1 Hz to 50 Hz. The shaking table has a base plate measuring 1 m × 0.8 m the maximum displacement capacity of the vibrating table was extended to ±250 mm. In this study, the total weight of the stack, sand, and pile with the pile cap, including the machine foundation, was 9kN. The servomotor of the shake table was controlled by a controller capable of generating sine waves and real-time historical data to drive the shake table.



(a)



(b)

Figure 1. Photograph of shaking table test component (a) Laminar shear box and machine foundation model; (b) Shaking table control and data acquisition hardware

2.2. Laminar Soil Container

The laminar soil box is designed to simulate seismic wave propagation within a finite soil layer [45–48]. It consists of 16 aluminum frames, each with a 40 × 40 mm cross-section, bolted together to form a rectangular container measuring 950 mm x 800 mm x 800 mm. The frames can move unidirectional and are separated by slide ball bearings, allowing relative movement up to ±150 mm, as shown in Figures 1 and 2. All laminae within the experimental apparatus were permitted unrestricted movement in the shaking direction, except the base lamina, which was rigidly fixed to the steel plate of the shaking table to simulate bedrock conditions. The mass of the container is 2.7% of the total soil mass. Tests are conducted at room temperature (25 °C). The rigid base of the stack was roughened using coarse sand to prevent the sand mass from sliding. A latex membrane was applied to the inside surface of the longitudinal walls of the stack. The latex membrane allows the soil to move freely in the longitudinal direction; similar arrangements have been reported in the literature [34, 46-52]. According to previous studies [53-57], the lateral boundary of the soil container should extend to at least 15D (D: pile diameter) (currently 22.5D) from the side of the system, and the vertical influence zone beneath the pile tip should extend to at least 10D (currently 22D). These criteria were satisfied in the present study.

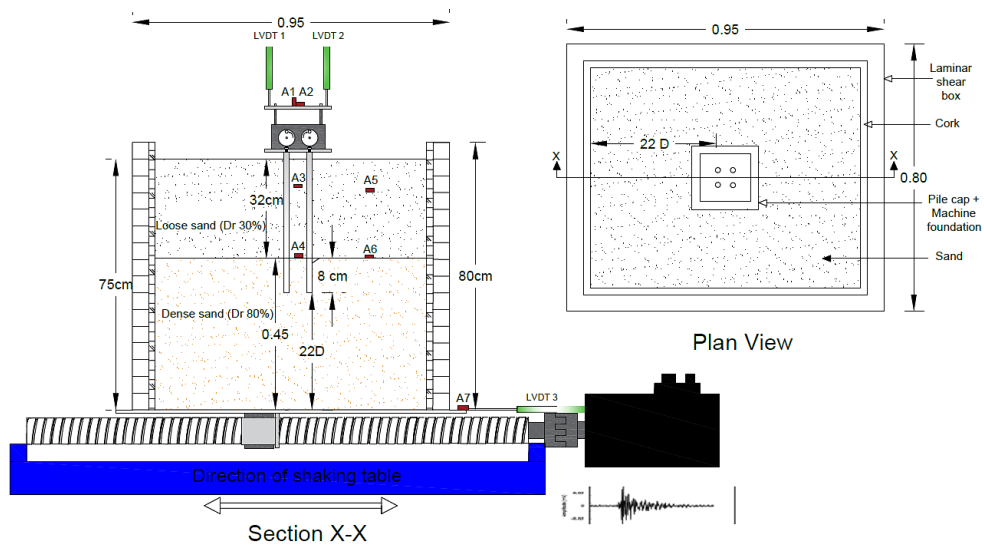


Figure 2. Schematic shaking table, test setup of, accelerometers, piles, pile cap, and machine foundation

2.3. Sensors Arrangement

Figure 2 illustrates the sensor arrangement employed during the vibration table test, providing both lateral and vertical perspectives of the monitoring zone. Data acquisition was achieved using a National Instruments (NI) system operating

at a sampling rate of 40,000 Hz. To capture the acceleration of the machine foundation, accelerometers A1 (the Bosch Piezoelectric Vibration Sensor (Model: 0 261 231 007)) and A2 were strategically positioned along the x (parallel to wave propagation) and z (vertical axes), respectively. An additional four accelerometers (A3, A4, A5, and A6) were installed within and adjacent to the pile assembly to assess the acceleration profiles at both near- and far-field locations. The shaking table was equipped with an accelerometer to record the input wave characteristics. The specifications of the sensors used in this study are listed in Table 1.

Table 1. Sensor Specifications

Sensor	Measurement Type	Code name	Specifications
Piezoelectric Vibration Accelerometer	Acceleration (g)	A1	Bosch Model: 0 261 231 007; Sensitivity: 15 mV/g;
Accelerometer	Acceleration (g)	A2-A7	Model: ADXL335; Sensitivity:300mV/g
LVDT	Displacement (mm)	LVDT 1-3	Model: (KTC-500); Linear accuracy :0.1%-0.05%

2.4. Similarity Ratio

The experimental model employed in this study was based on the scaling factors [45], as detailed in Table 2. The model piles consisted of hollow circular aluminium pipes with an outer diameter of 16 mm and a wall thickness of 1.2 mm with a young's modulus of 67GPa and 400-mm-length which corresponds to a prototype of a 300-mm-diameter concrete pile with a young's modulus of 25GPa and 7.5-m-length [34, 58]. To prevent soil intrusion, the bottoms of the hollow pile columns were capped with 3-millimeter aluminum plates. The upper layer is loose soil of Dr 30% and the bottom layer is dense soil of Dr 80%. The piles were inserted into the dense layer up to 8 cm (5D, as reported by Das & Sivakugan [59] to represent end bearing). A 1/10 scale model was selected due to the constraints of the apparatus of machine. In which applying the frequency scaling factor (model/prototype = 3.16), a prototype frequency of 30 Hz translates to 94.8 Hz in the model. Given that the max operating frequency of machine is up to 120 Hz, the 1/10 scale ensures that the machine can achieve the required frequencies. A schematic diagram of a group of piles with machine foundation and pile cap setup is shown in Figure 2. The amplitude scaling was derived based on the scaled frequency. When projecting the scaled frequency onto the chart for the prototype in ACI 351-3R-18 [60], it is imperative to employ the scaled model frequency. The author-derived displacement amplitude scaling equation is as follows:

$$Amplitude_{model} = \frac{Amplitude_{prototype}}{n^{2\alpha}} \quad (1)$$

where n is the scaling factor, and (α) is the scaling exponent related to frequency scaling. In existing literature, values for α typically range between 0.5 and 0.75 [61, 62].

Table 2. Scaling factor utilized in the shaking table for some variable as per [45]

Property	Quantity	Symbol	Formula	Scaling factors (Model/Prototype)
Geometry	Length (l)	Sl	Sl	1/10
	Linear Displacement (r)	Sr	$Sl^{-1} \cdot S\epsilon$	1/10
	Strain (ϵ)	$S\epsilon$	/	1
	Mass (M)	SM	$SM \cdot Sl^3$	0.001
	Density (ρ)	$S\rho$	/	1
	Stress (σ)	$S\sigma$	/	1
	Poisson's ratio (μ)	$S\mu$	/	1
Dynamic	EI	SL	$Sl^5 \cdot S\rho / S\epsilon$	100000
	Acceleration(a)	Sa	Sa	1
	Frequency (f) ($\alpha=0.5$)	Sf	$Sl^{-\alpha} \cdot Sa$	3.16
	Amplitude (mm) (current study)	Sn	$Sl^{2\alpha} \cdot Sa$	0.1
	Velocity (V)	Sv	Sv	1
	Time	St	$Sl^{0.5} \cdot S\epsilon$	0.316

2.5. Soil Model Utilized in the Study

The sand used in this study was locally sourced from Karbala, Iraq, and thoroughly cleaned and dried before testing. The soil was then poured into the model box in 10 cm thick layers using tamping to achieve a dense state of 80% Dr. After each layer was added, the surface was leveled using a steel board. To create a loose state, the upper layer of soil was deposited using air pluviation from a traveling hopper at a specified height. Soil samples were collected and

measured to ensure consistency across the layers. The properties of the tested soils are listed in Table 3. According to the Unified Soil Classification System (USCS), the soil was classified as poorly graded sand, as shown in Figure 3.

Table 3. Soil physical characteristic

Characteristic	Value	Standard
D10, D30, D60 (mm)	0.16, 0.25, 0.41	
curvature coefficient (Cc)	0.84	
Uniformity coefficient (Cu)	2.35	ASTM D422-02
Percentage Passing Sieve No. 200	0.58	
Soil Classification According to USCS	SP	
Specific gravity (Gs)	2.68	ASTM D 854
Maximum density (γ_d max) (kN/m ³)	18.55	ASTM D 4253-00
Minimum density (γ_d min) (kN/m ³)	15.85	ASTM D 4254-00
Density in loose state (30%) (kN/m ³)	16.67	
Density in dense state (80%) (kN/m ³)	18.03	
Internal Friction Angle (ϕ) in Dry State	36	ASTM D 3080

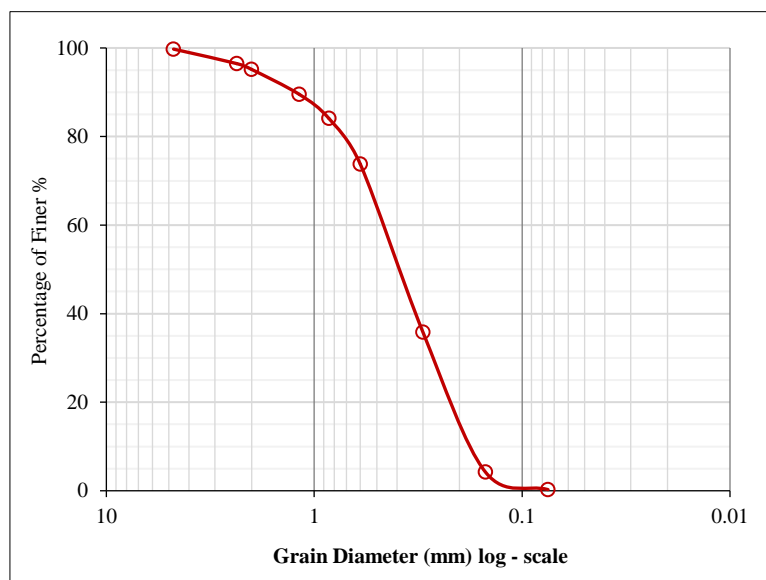


Figure 3. Particle size distribution of the tested soil

2.6. Testing Program

2.6.1. System Setup

The model has steel plates sized 200 mm by 200 mm by 8 mm to represent the machine foundation bolted on pile cap, which has the same thickness (8 mm) but dimensions of 150 mm by 150 mm. The pile cap was positioned 40 mm above the soil surface and bolted to a group of four piles; the group of four piles with spacing of 5D was employed based on ACI 351-3R [60]. The calculated foundation-to-machine mass ratio of 3.5 exceeded the minimum code-specified requirement outlined in ACI 351.3R-18. The vertical load was simulated by two DC spindle motors with an eccentric mass of 5 g and an eccentric distance of 25 mm in each motor for the opposite direction. Each motor has two eccentric masses, so the total mass will be 20 g in the whole system machine. As revealed in Figure 4, a special technique for rotating two motors using plastic gear to keep the two motors rotating in the reverse direction is placed inside a steel closed box that contains oil filled to 25% of its height. That would help to reduce friction and noise due to high-speed operation and facilitate the interaction between the two plastic gears. The principle of the rotating mass-type oscillator is mentioned in the literature [63, 64]. The amplitude of the vertical force generated is:

$$F_0 = m_e e \cdot \omega_n \quad (2)$$

where ω_n represent the dynamic force circular frequency (rad/sec), m_e represent the mass laid on disk (gram), and e represent the eccentric distance of mass (mm). The harmonic vertical mode of vibration for this kind of oscillator has a sinusoidal function. As a result, the dynamic force that is being applied at any time (t) is given by:

$$F(t) = F_0 \sin \omega_n t \tag{3}$$

The reliability of the piled machine foundation was ensured by conducting a single pile load test prior to the testing program, which confirmed that the load-carrying capacity of the system, with a factor of safety (FOS) of 4, met the design requirements.

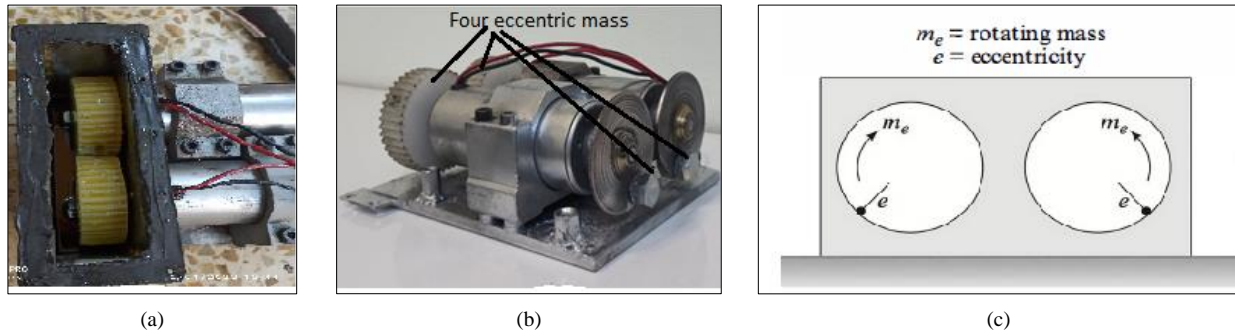


Figure 4. Model of vertical vibration: (a) Two plastic gears, (b) An overview (current study), and (c) Principle of Rotating mass-type excitation [63, 65]

2.6.2. Frequency and Amplitude Selection

The selection of operating frequencies and displacement amplitudes follows the recommendations of ACI 351-3R [60], using Richart et al. [66] and Blake charts as modified by Arya et al. [41] and ACI 351.3R [60] to determine the allowable vertical vibration amplitudes. A speed control unit is required to induce vibrations. The speed of the oscillator can be varied by varying the voltage supplied to the motor, and is regulated by the speed control unit, thereby modulating the frequency of the vibration induced by the oscillator. To measure the frequency, a tachometer was connected to a mechanical assembly fixed to the disc oscillator. This oscillator induces a force that is frequency-dependent for a given mass. Even at the same frequency, the amplitude of dynamic force can be changed by manipulating the mass (m_e) using external control. The scaling law was applied to convert the three prototype frequencies (10, 20, and 30 Hz) into model frequencies of 31.6, 64.2, and 94.8 Hz, respectively. Figure 5 shows the variation in the amplitude with frequency by changing the operating frequency of the machine, with each stage lasting for at least 60 s to observe the amplitude changes and determine the resonant frequency of the system. Figure 5-a shows the selected model frequency, and Figure 5-b shows the frequency ratio of the system, presenting the resonant regions and the high- and low-tuned frequencies. Notably, the frequencies were strategically selected to remain outside the resonant range.

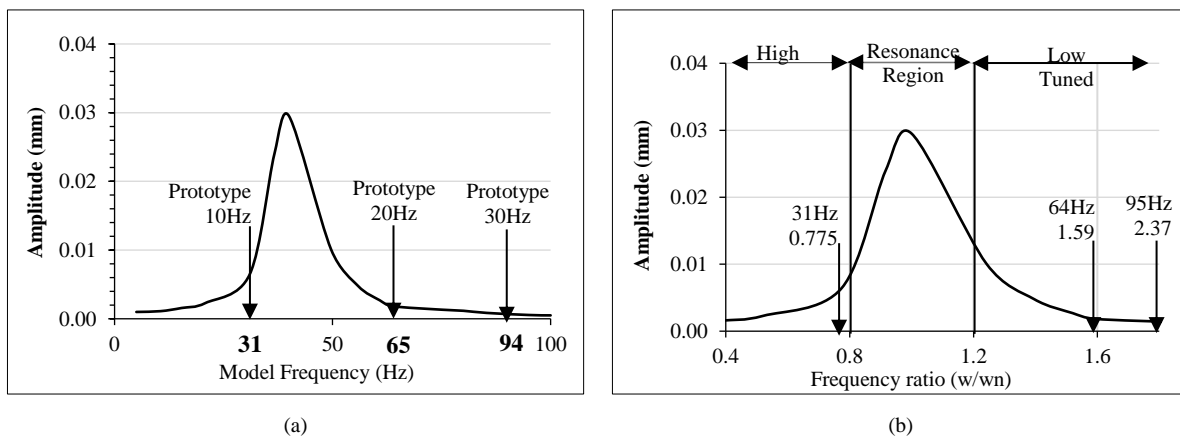


Figure 5. Variation of Amplitude with Frequency: (a) Amplitude vs. frequency, (b) Frequency Ratio and Resonance Regions

2.6.3. Classification of Frequencies

Amplitude scaling was performed prior to frequency classification. By projecting the selected frequencies onto charts, the frequencies can be classified according to machine severity and vibration criteria. As shown in Figure 6-a, the frequencies of 10 Hz and 20 Hz fall within the (good) region, and the frequency of 30 Hz is in the (very good) region. In parallel, in Figure 6-b, the frequency of 10 Hz is in (Region B), and the frequencies of 20 Hz and 30 Hz are in (Region A).

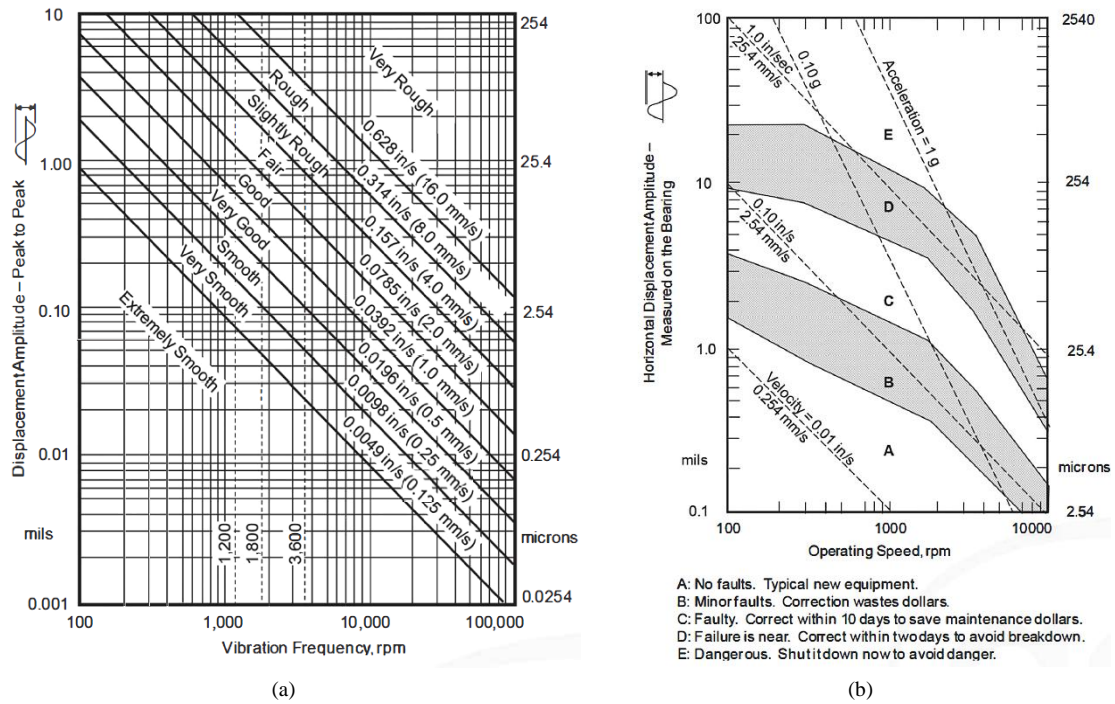
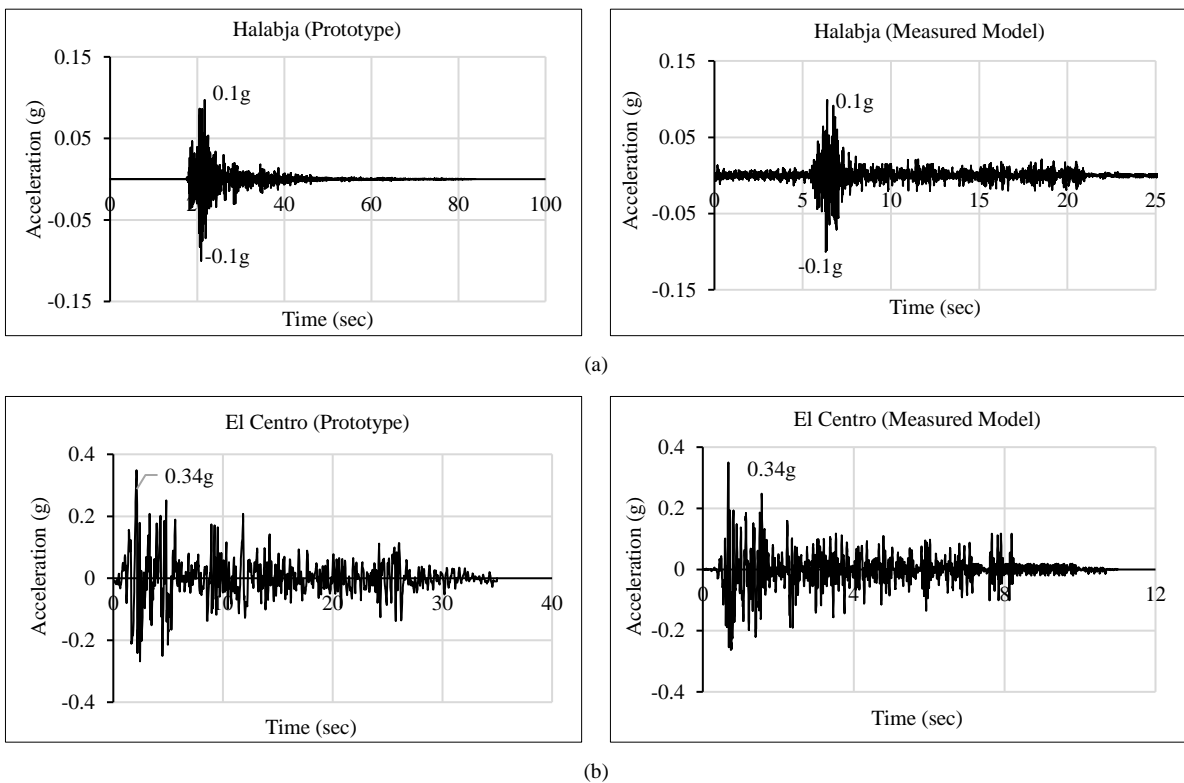


Figure 6. Allowable vertical displacement amplitude of selected frequencies: (a) Vibration Severity Chart, (b) Criteria of vibration for rotating machinery [41, 60] (Note: One mil equals 0.001 inches).

2.6.4. Selection and Scaling of Seismic Input Motions for Experimental Analysis

The prevailing approach to scientific research in this field involves the use of historical earthquake records [67]. The machine was operated for 10 min at each frequency before being subjected to four earthquake excitations. Halabja, El-Centro, Kahramanmaras, and Kobe were selected as the input ground. The time of earthquake ground motion was scaled by a factor of 3.16. The scale factor should typically range from (2-4 to), as reported by [49, 67, 68] to avoid unrealistic ground motion. The model earthquake records and details are listed in Table 4 and depicted in Figure 7. The testing program, detailed in Table 5, consists of 12 tests across three distinct phases.



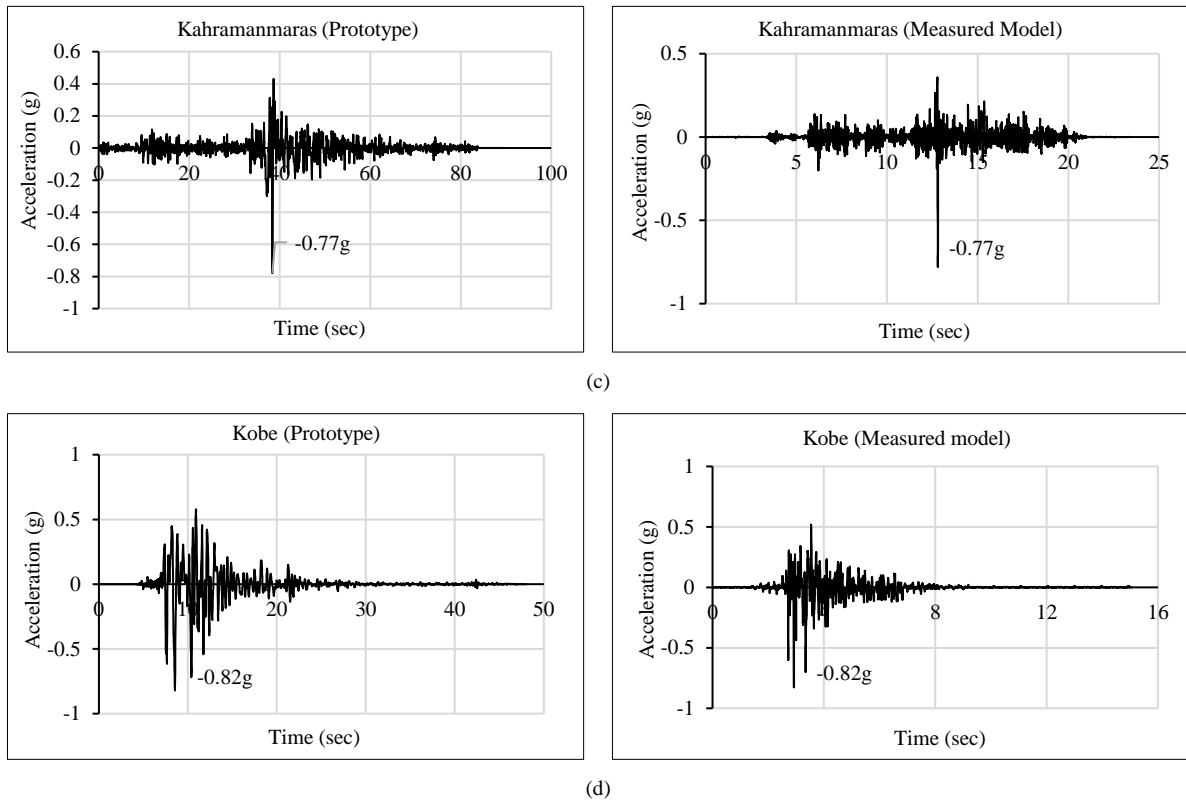


Figure 7. Time histories of prototype earthquake and model signals inputted to shaking table: (a) Halabja, (b) El Centro, (c) Kahramanmaras, (d) Kobe

Table 4. Overview of seismic event data

Parameter	Halabja	El-Centro	Kahramanmaras	Kobe
Geographical Area	Iraq-Iran Border	California, USA	southern Turkey	Japan
Recorded Date (in UTC)	2017-11-12 18:18:17	1940-05-19 04:36:41	2023-02-06 01:17:34.342 UTC	1995-01-16 20:46:52
Magnitude (Mw)	7.3	6.9	7.7	6.9
Duration of Tremors (seconds)	84	35	125	48
Peak Ground Acceleration (g)	East-West	North-South	East-West	North-South
Depth of Epicenter (km)	19	8.8	8.6	7.9
Distance to Epicenter (km)	218.8	12.2	106.49	1.0
Reference	Iraqi Meteorological Seismology [69, 70]	[71]	AFAD [35, 72]	[73]

Table 5. Testing program overview: vibration frequencies and seismic events

Test No.	Initial vibration (Hz)	Seismic event
1	10	Halabja (0.1g)
2	10	El Centro (0.34g)
3	10	Kahramanmaras (0.77g)
4	10	Kobe (0.82g)
5	20	Halabja (0.1g)
6	20	El Centro (0.34g)
7	20	Kahramanmaras (0.77g)
8	20	Kobe (0.82g)
9	30	Halabja (0.1g)
10	30	El Centro (0.34g)
11	30	Kahramanmaras (0.77g)
12	30	Kobe (0.82g)

3. Result and Discussion of Acceleration Response of Piled Machine Foundation

3.1. Effect of Varying Frequency under Earthquake Excitation

The input motion propagates through the soil layers. It undergoes amplification or attenuation at the ground surface based on the dynamic properties of the soil column and the frequency content [74-76]. Figure 7 presents a comparative analysis of the representative time histories and their corresponding peak ground accelerations (PGA) measured using two accelerometers (HA and VA) attached to the machine foundation surface at operating frequencies of 10, 20, and 30 Hz. Each frequency was subjected to maximum shaking accelerations of 0.1 g (Halabja), 0.34 g (El Centro), 0.77 g (Kahramanmaras), and 0.823 g (Kobe). The results were obtained at a fixed pile spacing of 5D under dry conditions. These figures illustrate three phases:

- **Initial vibration:** This phase represents the regular operation of machine which lasts for 20 minutes and only a few seconds are shown in the figures.
- **Seismic event:** The system was subjected to an earthquake (input motion).
- **Recovery phase:** This represents the period after the earthquake ends (post-earthquake).

As illustrated in Figure 8-a to 8-d, the average time history response of the acceleration exhibits nonlinear behavior. In this case, the HA can amplify from 0.1 g and 0.34 g to 0.29 g and 0.43 g due to the high shear modulus of the soil, which provides greater rigidity and less damping, thus allowing greater energy to be transferred and motion amplification [77].

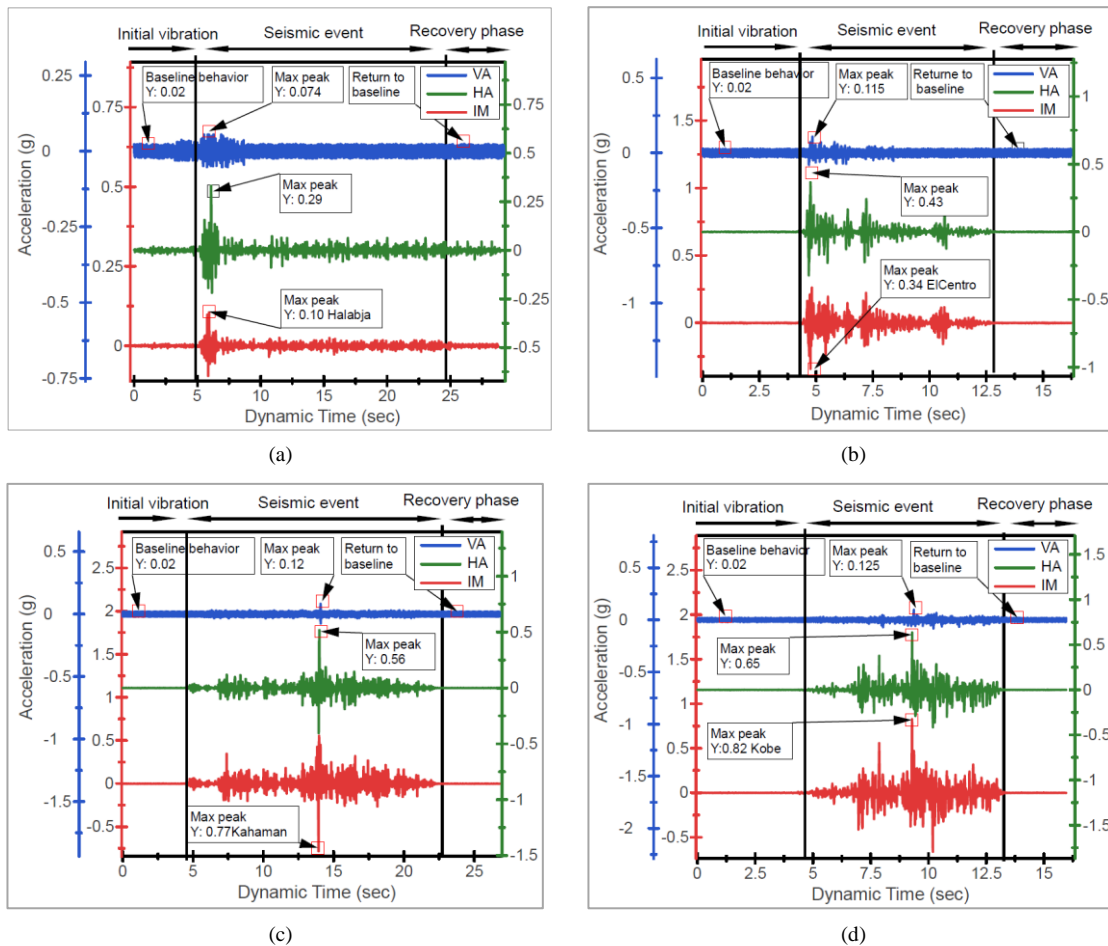


Figure 8. Acceleration response of piled machine foundation at 5D spacing and 10 Hz under various earthquake intensities: (a) 0.1g Halabja, (b) 0.34g El Centro, (c) 0.77g Kahramanmaras, (d) 0.82g Kobe

In the case of higher input acceleration, the HA of 0.77 g and 0.82 g are reduced to 0.56 g and 0.65 g, respectively, due to the soil undergoing plastic deformation or partial shear failure, the shear modulus decreases and the material damping increases, resulting in more energy absorption and reduced wave transmission. The same trend in Figure 9, the HA amplified to 0.25 g at an input acceleration of 0.1 g and reduced to 0.33 g, 0.5 g, and 0.58 g at input acceleration of 0.34 g, 0.77 g, and 0.823 g, respectively.

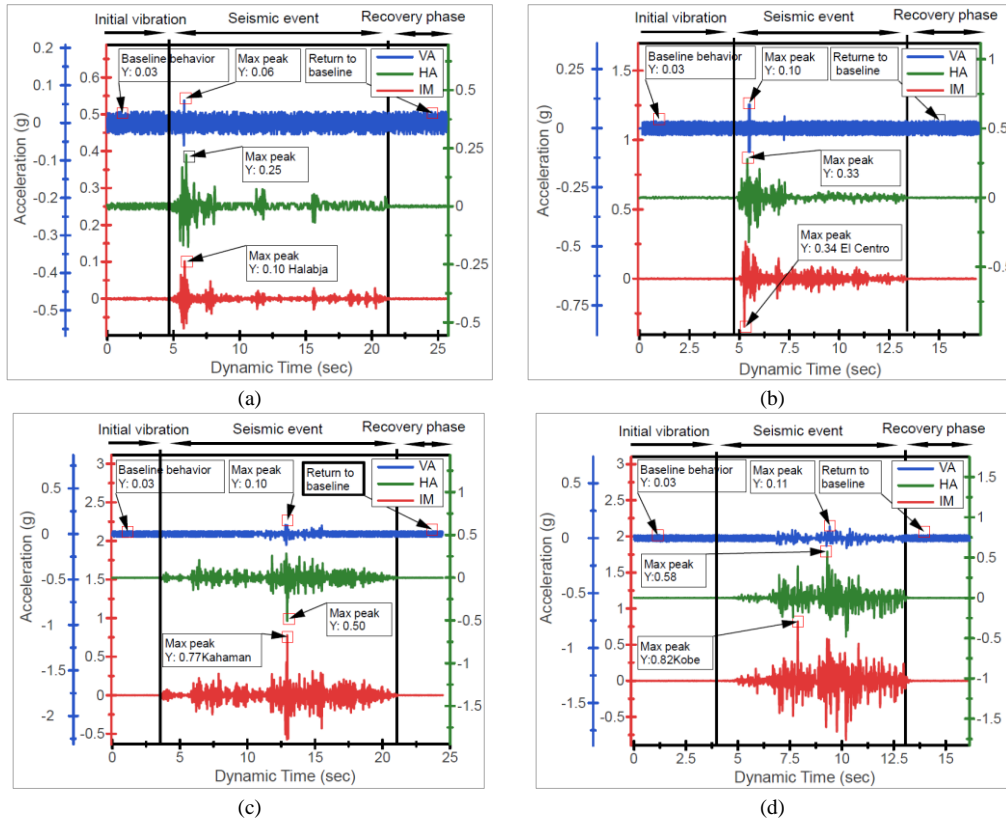


Figure 9. Acceleration response of piled machine foundation at 5D spacing and 20 Hz under various earthquake intensities: (a) 0.1g Halabja, (b) 0.34g El Centro, (c) 0.77g Kahramanmaraş, (d) 0.82g Kobe

As shown in Figures 11-a and 11-b, the general pattern indicates that HA and VA are directly proportional to the increase in the frequency. The HA increased by 129%, 132%, and 168% for 10 Hz, 20 Hz, and 30 Hz, respectively, with increasing input shaking accelerations from 0.1 g to 0.82 g, respectively. In parallel, the VA shows an increase of 68%, 100%, and 125% for 10 Hz, 20 Hz, and 30 Hz, respectively, with increasing input shaking acceleration from 0.1 g to 0.82 g, respectively.

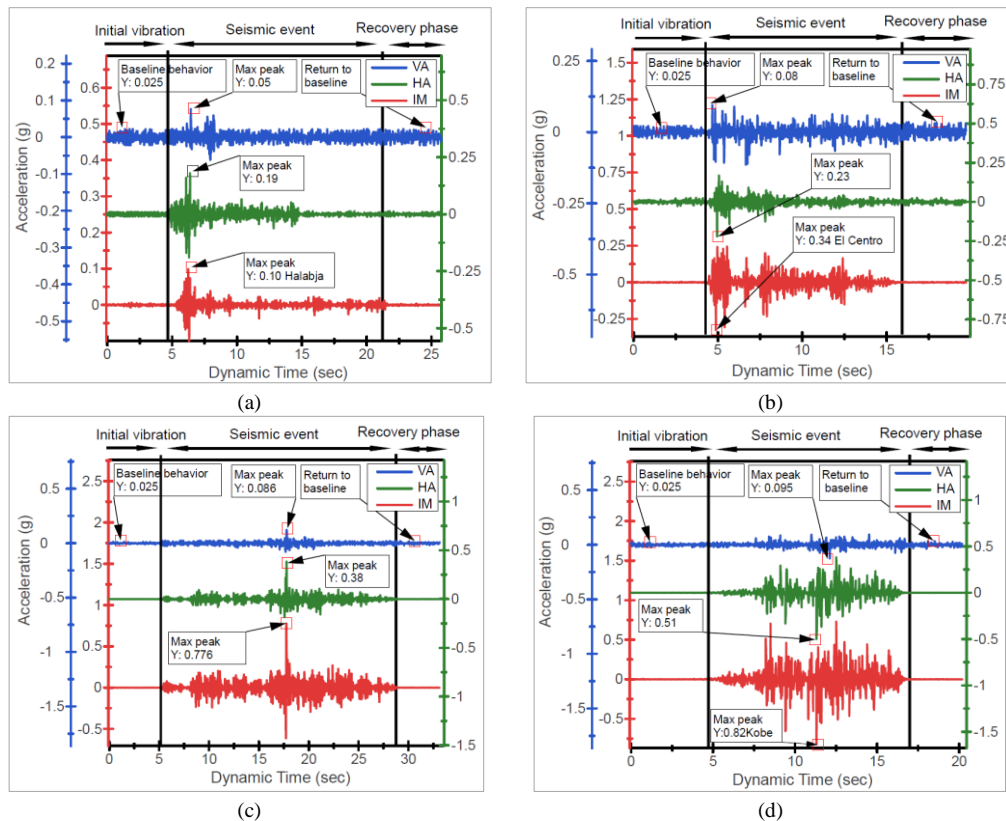


Figure 10. Acceleration response of piled machine foundation at 5D spacing and 30 Hz under various earthquake intensities: (a) 0.1g Halabja, (b) 0.34g El Centro, (c) 0.76g Kahramanmaraş, (d) 0.83g Kobe

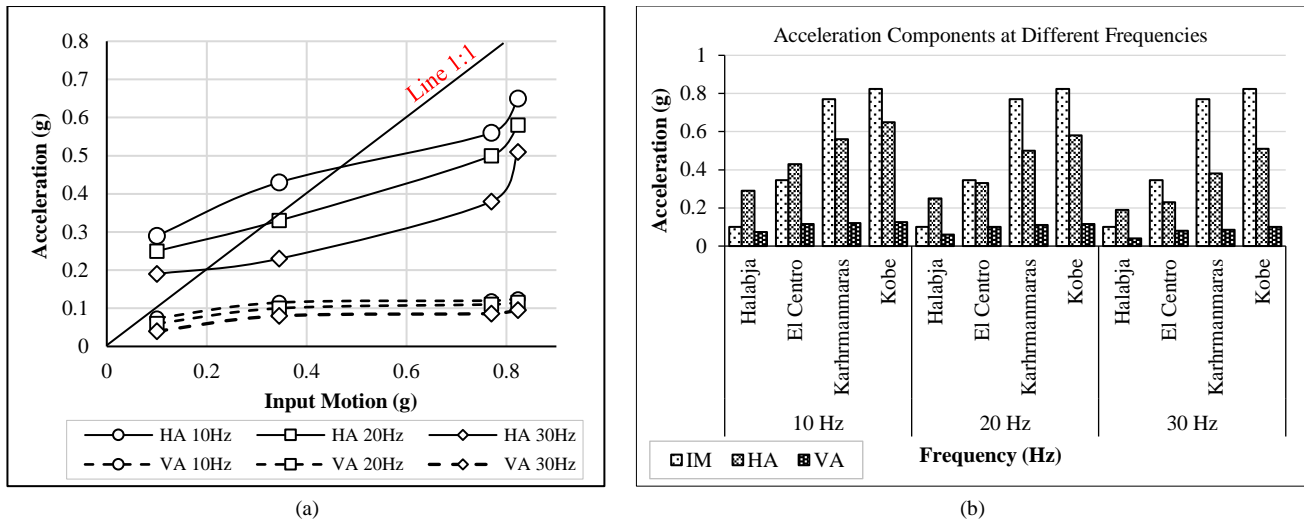


Figure 11. Comparison of (a) horizontal and vertical acceleration across different intensities and (b) the effect of frequency variation on earthquake-induced accelerations

This reduction is due to the increased system stiffness at higher frequencies, which reduces vibration amplitudes. Additionally, higher frequencies enhance energy dissipation through material and radiation damping, and the gyroscopic effects of rotating machinery further reduce horizontal accelerations.

3.2. Amplification Ratios

3.2.1. Horizontal Amplification Factor (HAF)

The HAF is defined as the ratio of the horizontal acceleration response to the horizontal input motion as follows:

$$HAF = \frac{\text{Horizontal Acceleration Response}}{\text{Horizontal Input Motion}} \tag{4}$$

Figures 12-a and 13 show that the HAF exhibits attenuation, which increases with increasing frequency. HAF showed an attenuation of 2.9 times at 10 Hz and 1.9 times at 30 Hz for 0.1 g. As the input motion increased to 0.34 g, the HAF at 10 Hz showed a significant reduction of approximately 47%. This reduction trend continues with a further increase in seismic intensity up to 0.82 g. However, this reduction increases slightly with increasing frequency but remains less than one except at 0.34 g, where the HAF shows an amplification of 1.25 times at 10 Hz. Figure 13 shows that the HAF increased by 34%, 47%, 32%, and 22% for input shaking accelerations of 0.1 g, 0.34 g, 0.77 g, and 0.82 g, respectively, when frequency increased from 10 Hz to 30 Hz.

In addition, the observed results, as shown in Figure 12-a for the HAF, indicate that as the frequency increases, the damping effect increases significantly, reaching a maximum reduction at 30 Hz, especially for 0.34 g, 0.77 g, and 0.82 g. This phenomenon can be explained by the properties of the interaction between the soil and mechanical damping dynamics. Higher frequencies correspond to shorter wavelengths in the seismic waves. As the wavelength becomes shorter, the waves tend to interact more with the pile group as a whole rather than individual piles, reducing the amplification effects seen at lower frequencies. This results in lower acceleration levels at higher frequencies [78, 79].

Furthermore, the reduction in horizontal acceleration (HA) can be attributed to the frequency-dependent behaviour of pile stiffness and damping, which become more effective at higher frequencies. As frequency increases, the system's stiffness enhances, and the damping mechanisms become more efficient in dissipating energy. Which may attribute to higher frequencies result in a greater conversion of the soil material damping (β) and frequency (ω) into an equivalent viscous damping coefficient, reducing vibration amplitudes and subsequently lowering accelerations, as reported by Garala & Madabhushi [52] and Manna & Baidya [80]:

$$C = \frac{2\beta}{\omega} \tag{5}$$

3.2.2. Vertical Amplification Ratio (VAR)

Since vertical vibration (amplitude of acceleration) is measured in the vertical direction and may amplify during an earthquake, this ratio may be called the vertical amplification factor (VAF). VAF is defined as the ratio of the vertical acceleration response during the earthquake to the vertical acceleration before the earthquake, as follows:

$$VAF = \frac{\text{Max peak of VA during earthquake}}{\text{Initial VA before earthquake}} \tag{6}$$

The VAF in Figures 12-b and 13 shows nonlinear behavior, but decreases with increasing frequency. VAF decreased by 32%, 13%, 10%, and 5% for 0.1 g, 0.34 g, 0.77 g, and 0.82 g, respectively, when frequency increased from 10 Hz to 30 Hz. As the operating frequency of the rotating machine increases, the displacement amplitude decreases. Despite a decrease in the displacement amplitude with increasing frequency, the dynamic force associated with the high-frequency machine vibrations was amplified. This can be explained by the basic principles of vibration and dynamics [63, 81-83]. The following relationship expresses the dynamic force generated by the rotating machine:

$$F_{Dynamic} = 2\pi f \times A \tag{7}$$

where: $F_{Dynamic}$: dynamic force (N), f : is the operating frequency (Hz), A : is the amplitude of the vibration (mm).

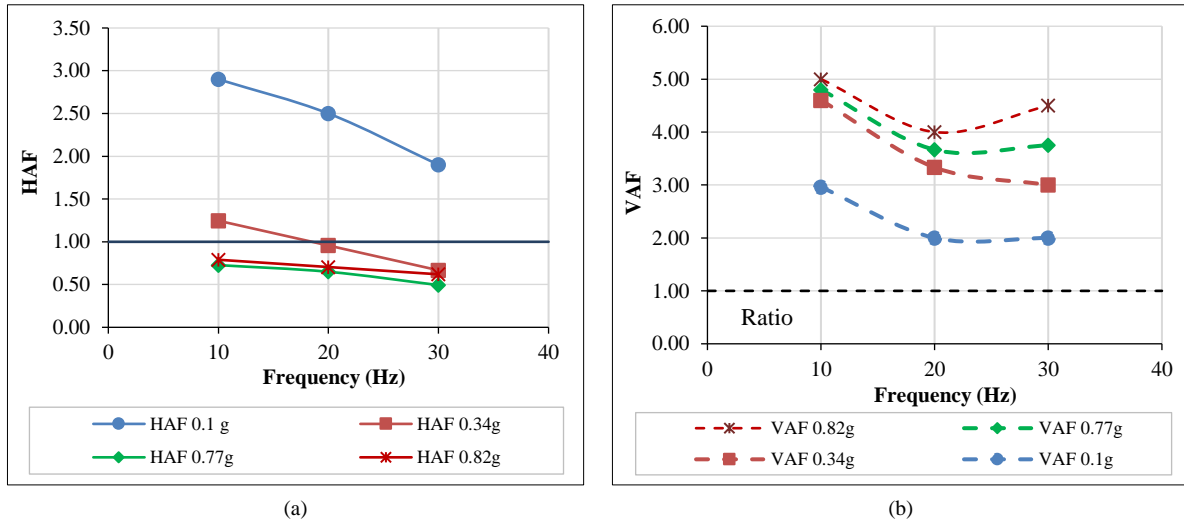


Figure 12. Variation of HAF and VAF as a function of frequency under different earthquake, (a)HAF, (b)VAF

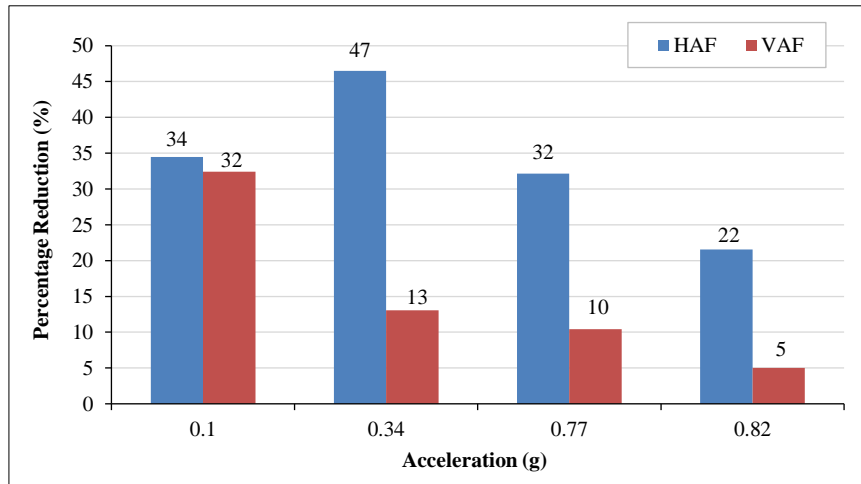


Figure 13. Percentage change in amplification factors from 10Hz to 30Hz for different earthquakes

As shown in Figures 12-a and 13, the vertical vibrations (VA) induced by the machine can reduce the horizontal amplification in the system through the following mechanisms:

- First, vertical vibrations destructively interfere with horizontal seismic waves, thus reducing the overall amplitude; such evidence was reported by Crouse & Jennings [84], Wolf [85] that for specific wavelengths (λ) and angles of incidence (α), the ground beneath the building tends to move in opposite directions. The concept of wave filtering by the foundation is illustrated in Figure 14 The ground beneath the building tends to move in opposite directions. Owing to the high stiffness of the foundation, the wavelengths were effectively filtered. When waves hit the foundation, their energy is partially absorbed and redirected or reflected, thereby decreasing the amplitude of the horizontal motion transmitted to the building. Gazetas [86] observed that group piles could alter and reduce the seismic waves transmitted to the structure; at high frequencies, the group piles may not be able to follow the wavy movement of the free field. Filtering or kinematic interaction, as described by Crouse & McGuire [87], is attributed to (1) seismic waves incident at angles less than 90° , and (2) spatial variability in ground motion due to wave scattering caused by geological heterogeneities and energy dissipation. In parallel, previous studies [88-91] observed that differential earthquake responses across foundation slabs with amplified ground motion at the points of later wave arrival, where the input wave reaches later, are more significant than at the other end.

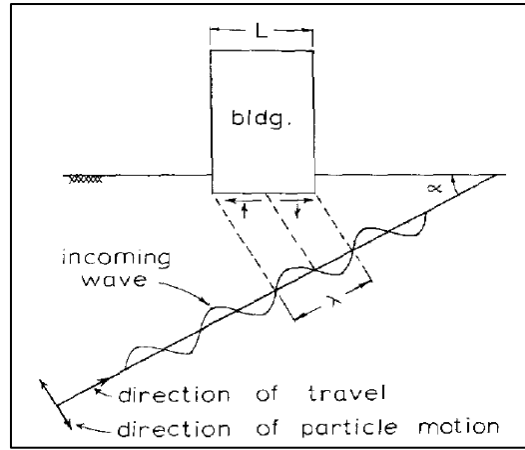


Figure 14. Filtering by foundation of a plane harmonic wave incident at an angle [84]

- Second, the interaction between soil structures can dissipate energy as vertical movements change the proportion of the horizontal movement of the ground and can lead to the creation of shear forces that dissipate energy through friction and hysteresis [85, 92-94]. However, this interaction helps destroy seismic energy more effectively, reducing amplification in the area adjacent to the piles. Therefore, continuing vertical vibrations provide stability by changing the resonance patterns and promoting continuous energy dissipation, which is consistent with the increased damping ratios and hysteresis behaviour in the soil during cyclic loading.
- Third, the inertia of the elevated cap plays a vital role in the dynamic behavior. The soils behaved elastically at low PGA levels (less than 0.1 g), increasing amplification. However, at PGA levels greater than 0.34 g, inertia can reduce the direct transmission of seismic waves from the soil to the foundation. The mass of the elevated cap and the rigidity of the machine foundation led to dynamic interactions that changed the natural frequency of the system, particularly shifting it away from the dominant frequencies of the seismic waves.

In the passive state, where the machine is off (zero Hz), as shown in Figure 14a, the piled machine foundation is subjected to an input motion to evaluate the typical response (reference) without the influence of the operating frequency. Observations indicated a significant reduction from the passive to the active state, especially at an operating frequency of 30 Hz. The reduction in horizontal acceleration (HA), called mitigation efficiency, represents the percentage reduction from the negative state (0 Hz) to other frequencies. The mitigation efficiency is quantified using the following equation:

$$ME = \frac{R_{static} - R_{dynamic}}{R_{static}} \times 100 \tag{8}$$

where ME is Mitigation efficiency, R static is Response without dynamic load, R dynamic is Response with dynamic load.

As illustrated in Figure 15-b, the mitigation efficiency increases with increasing peak ground acceleration, for instance, showing mitigation efficiency of 42%, 68%, 75%, and 63% at 30 Hz for earthquake intensities of 0.1 g, 0.34 g, 0.77 g, and 0.82 g, respectively. This shows that the mitigation efficiency is more effective at high frequencies. A similar trend was observed at 10 Hz and 20 Hz, but this trend decreased as the frequency decreased.

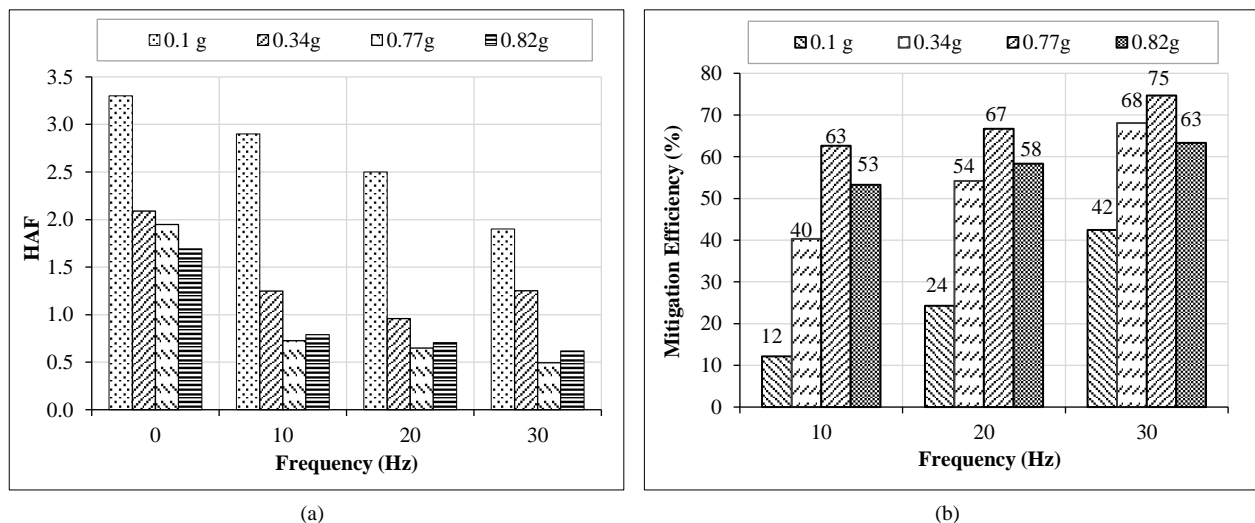


Figure 15. Analysis of amplification and vibration mitigation at various operating frequencies and Seismic Intensities: (a) HAF and, (b) Mitigation Efficiency (%)

3.2.3. Analysis of Displacement Amplitudes Relative to Vibration charts

The displacement amplitudes of the machine foundation system under various seismic intensities were analysed. The initial non-seismic condition (0 g) served as a baseline, adhering to the standard vibration limits outlined in the ACI 351.3R-18 charts. The results illustrated in Figures 16-a and 16-b are discussed below:

1. Displacement Amplitudes at 10 Hz:

The initial displacement amplitude fell within Zone B (Minor Faults), as shown in Figure 16-a. Under a seismic intensity of 0.1 g, the amplitude shifts to Zone C (Faulty), with a corresponding transition from the (Very Good) zone to the (Fair) zone on the vibration severity chart. At higher seismic intensities (0.34 g, 0.77 g, and 0.82 g), the amplitude shifts from Zone B to Zone D (Fault in Near) and from (Very Good) to (Slightly Rough) on the severity chart, as shown in Figure 16-b.

2. Displacement Amplitudes at 20 Hz:

The amplitude initially fell within Zone A (No Fault), as shown in Figure 16-a. Under a seismic intensity of 0.1 g, it shifts to Zone B (Minor Faults), with a corresponding move from the (Very Good) zone to the (Good) zone on the severity chart. At seismic intensities of 0.34 g, 0.77 g, and 0.82 g, the amplitude transitions from Zone A to Zones B-C (Minor Faults to Faults in Near) on Blake's chart and from Very Good to Good-Fair on the severity chart as shown in Figure 16-b.

3. Displacement Amplitudes at 30 Hz:

The amplitude remains within Zone A (No Fault) under seismic intensities of 0.1 g and 0.34 g. However, at 0.77 g and 0.82 g, it shifts from Zone A to Zone B, as shown in Figure 15a. On the severity chart, at 0.1 g, 0.34 g, and 0.77 g, the amplitude transitions from the Very Smooth-Smooth zone to the Very Good zone, except at 0.82 g, where it moves to the Good zone, as shown in Figure 16-b.

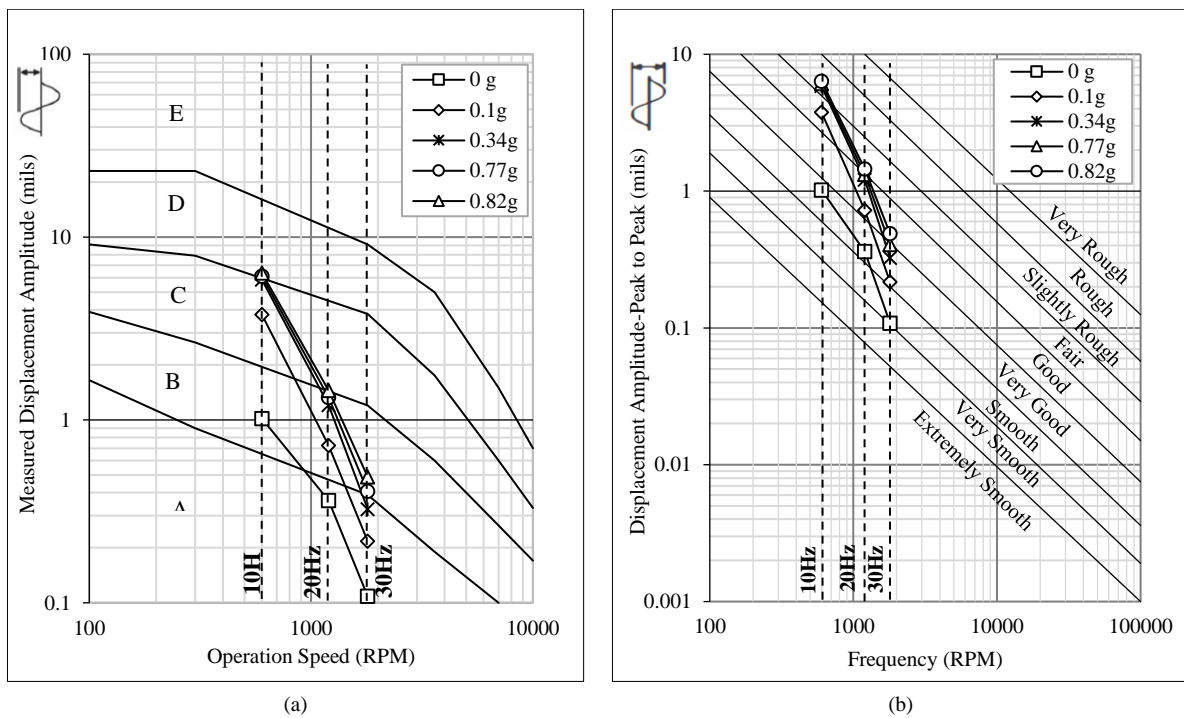


Figure 16. Extended vibration severity analysis under seismic loading: (a) Modified vibration criteria chart (ACI 351.3R-18 [60]), (b) Modified vibration severity chart (ACI 351.3R-18 [60])

3.3. Fast Fourier Transform and Spectral Acceleration Analysis

3.3.1. Fast Fourier Transform (FFT)

The frequency content characteristics of the acceleration response of a piled machine foundation subjected to three distinct operating frequencies under various seismic excitations were analyzed. Figures 17 and 18 illustrate the results of the Fast Fourier Transform (FFT) and spectral acceleration analyses performed on seismic signals from four prototype earthquake events. The original time-domain signals were scaled by a factor of 3.16, increasing their frequency content by the same factor when inputted into the shaking table. The resulting model signals were analyzed using FFT to identify and characterize the dominant frequencies.

Fast Fourier Transform (FFT) analysis of the Halabja earthquake signal identified dominant frequency components at 2.6 Hz and 6.7 Hz, as shown in Figures 17-a and 17-b. In contrast, the corresponding model signal exhibited 8.2 Hz and 21.2 Hz frequency peaks. The prototype signal revealed a dominant frequency of 1.46 Hz for the El Centro Earthquake. In contrast, the model displayed three peaks at 3.7 Hz, 4.63 Hz (dominant), and 7 Hz, as illustrated in Figures 18-a and 18-b. The prototype earthquake signal for Kahramanmaras showed dominant frequencies at 0.3 Hz, 0.8 Hz (dominant), and 2.34 Hz. However, the model exhibited a broader frequency spectrum, with peaks at 1, 2.5 Hz (dominant), and 7.4 Hz. The prototype signal displayed dominant frequencies at 1.4 Hz and 2.9 Hz for the Kobe earthquake, while the model indicated peaks at 1 Hz and 4.5 Hz (dominant).

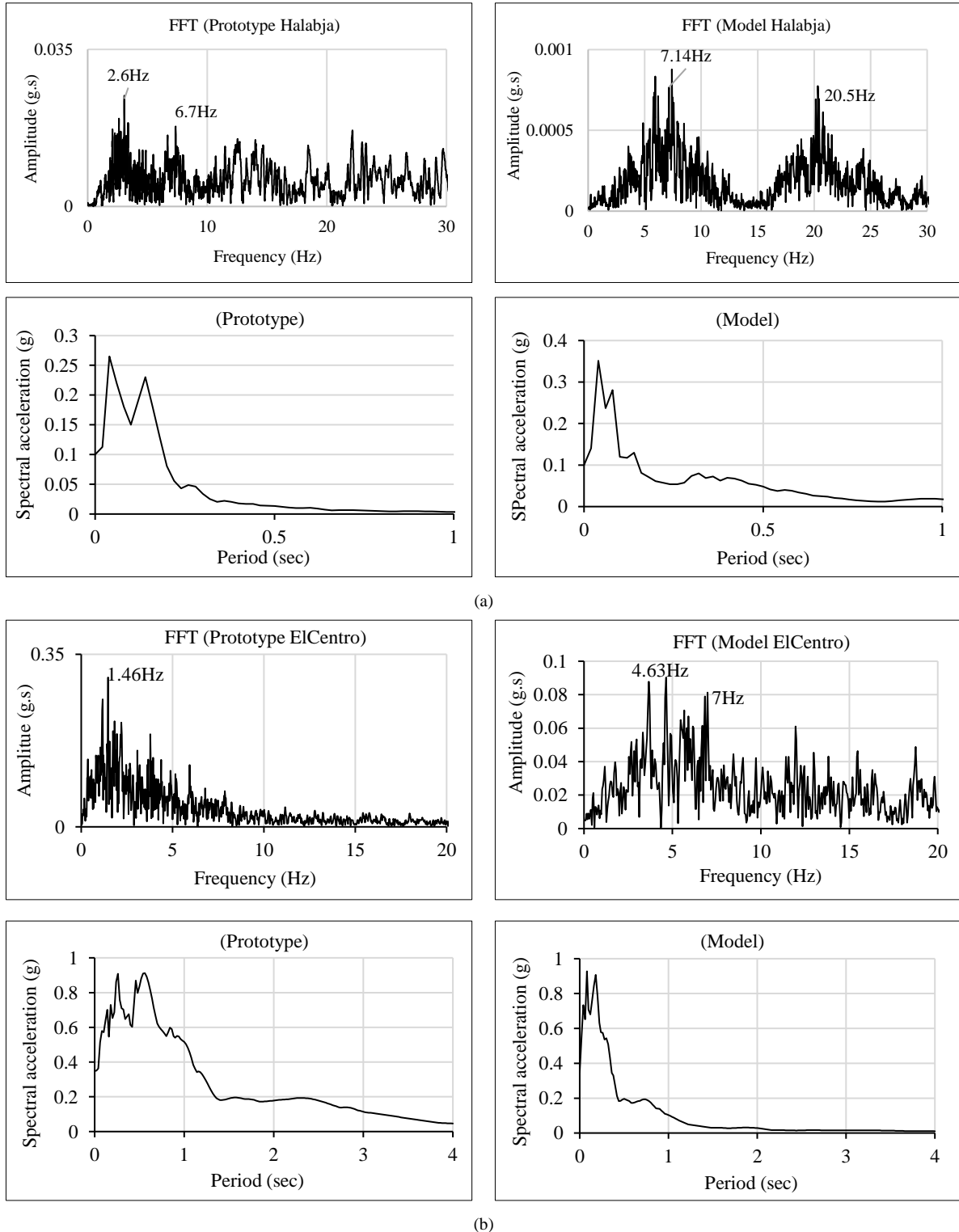


Figure 17. Time histories, frequency contents and spectral acceleration of prototype earthquake and model signals inputted to shaking table ($\zeta=5\%$):(a) Halabja, (b) El Centro

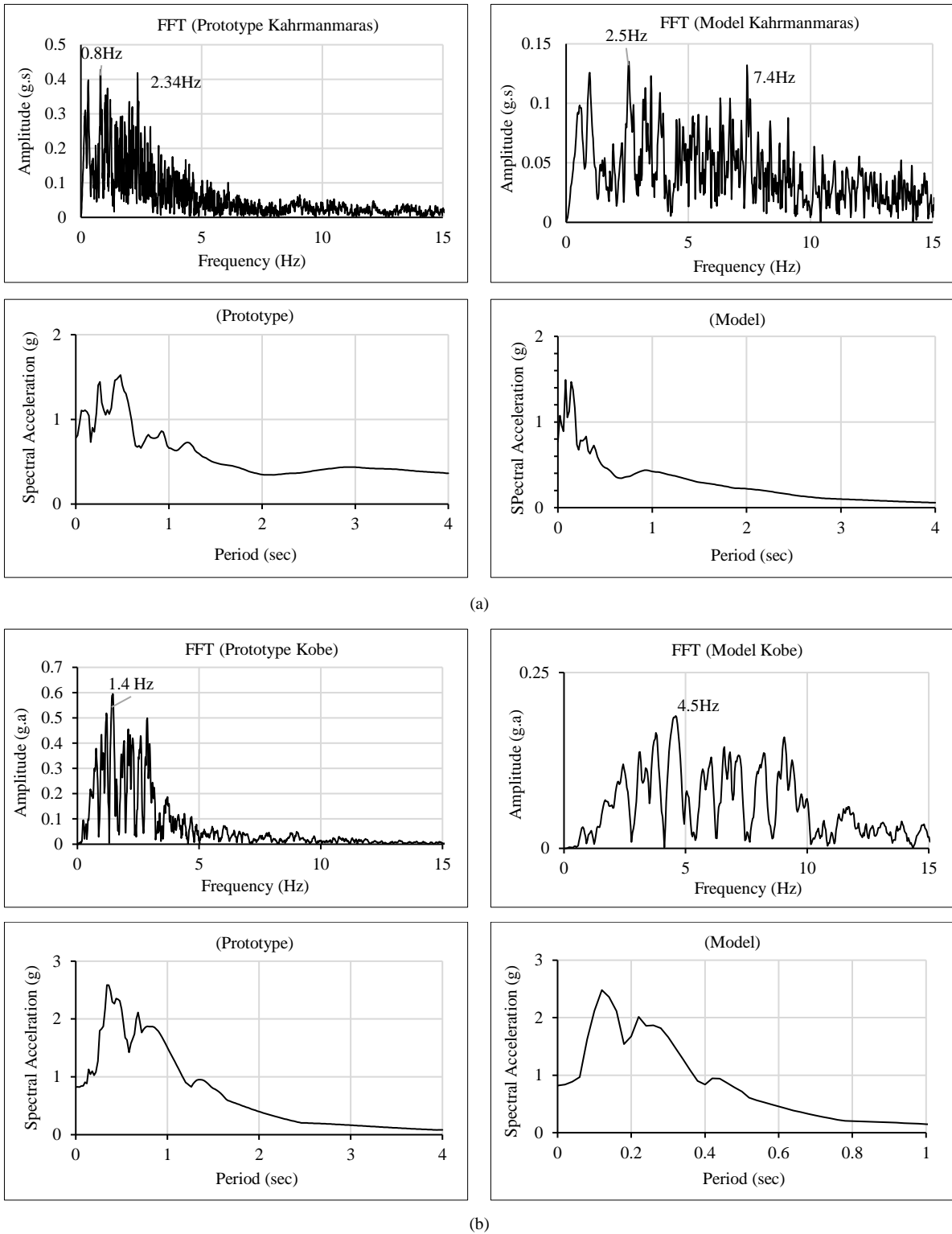


Figure 18. Time histories, frequency contents of prototype earthquake and model signals inputted to shaking table ($\zeta=5\%$): (a) Kahramanmaras, (b) Kobe

As illustrated in Figure 19, the frequency content of the piled machine foundation (5D spacing, 10 Hz) under various seismic intensities is analyzed as follows:

Halabja (0.1g): Fourier analysis reveals a prominent peak at approximately 7 Hz, attributed to soil resonance, with the Fourier amplitude being three times higher than the dominant frequency of the input motion. The vertical acceleration displays peaks at 3.6 Hz, 9.75 Hz, and 17 Hz, with the highest peak occurring at 10 Hz. This is likely due to the potential resonance within the piled machine foundation, where the Fourier amplitude slightly exceeds that of the input motion, indicating the presence of harmonic resonance. This suggests that vertical vibrations interfere with the vertically

propagating waves caused by horizontal motion [95]. Horizontal acceleration also exhibits multiple peaks, with the maximum occurring at 19.6 Hz, where the Fourier amplitude is 2.15 times greater than that of the dominant input motion frequency. This can be explained by the higher mode effects or interactions that induce significant responses at these frequencies, as shown in Figure 19-a.

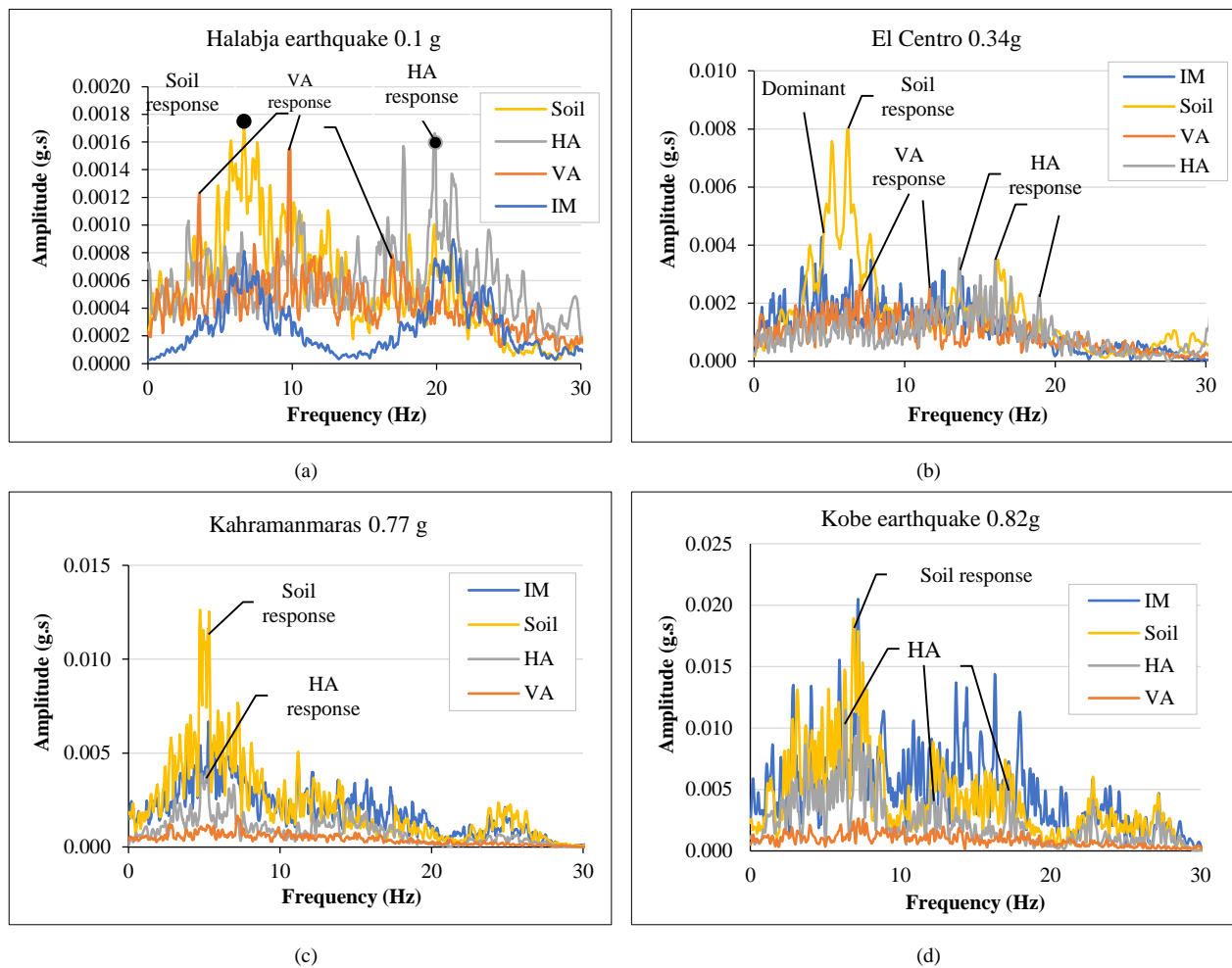


Figure 19. Frequency contents of piled machine foundation (5D,10Hz) under Various Intensities: (a) Halabja (0.1g), (b) El Centro (0.34g), (c) Kahramanmaraş (0.77g), (d) Kobe (0.82g)

El Centro (0.34g): As illustrated in Figure 19-b, the soil exhibits resonance between 5-7 Hz, with the maximum peak amplitude reaching twice that of the dominant input motion. The horizontal acceleration shows resonance with peaks at 13 Hz, 17 Hz, and 19 Hz, although each is lower than the amplitude of the input motion. The vertical acceleration resonates at 7 and 12 Hz; however, the peak amplitudes are less than those of the input motion.

Kahramanmaraş (0.77g): As shown in Figure 19-c, the soil also resonates at 5-6 Hz. The horizontal acceleration exhibited a peak in this frequency range, although the amplitude remained below that of the input motion. Beyond this range, the frequency component decreased. The horizontal acceleration slightly underperforms the dominant frequency before tapering off, whereas the vertical acceleration shows no resonance, indicating a minimal impact.

Kobe (0.82g): As shown in Figure 19-d, the soil resonates at 7 Hz, whereas the horizontal acceleration exhibits peaks at 7, 13, 17, and 23 Hz, with the most significant resonance occurring at 7 Hz. No substantial change in vertical acceleration was observed, indicating a limited vertical dynamic response.

As can be seen in Figure 20-a for Halabja (0.1g), Fourier analysis revealed that the soil resonated with a peak at approximately 7 Hz. The horizontal acceleration initially attenuates before showing multiple peaks at 6, 8, 10, 19, and 22 Hz, with the highest peak at 22 Hz amplified 1.5 times compared to the dominant input motion. The vertical acceleration resonates with a maximum peak at 19 Hz, slightly above the dominant frequency. This is likely because of the higher harmonic components of the input motion, which is consistent with the principles of wave interference and harmonic resonance.

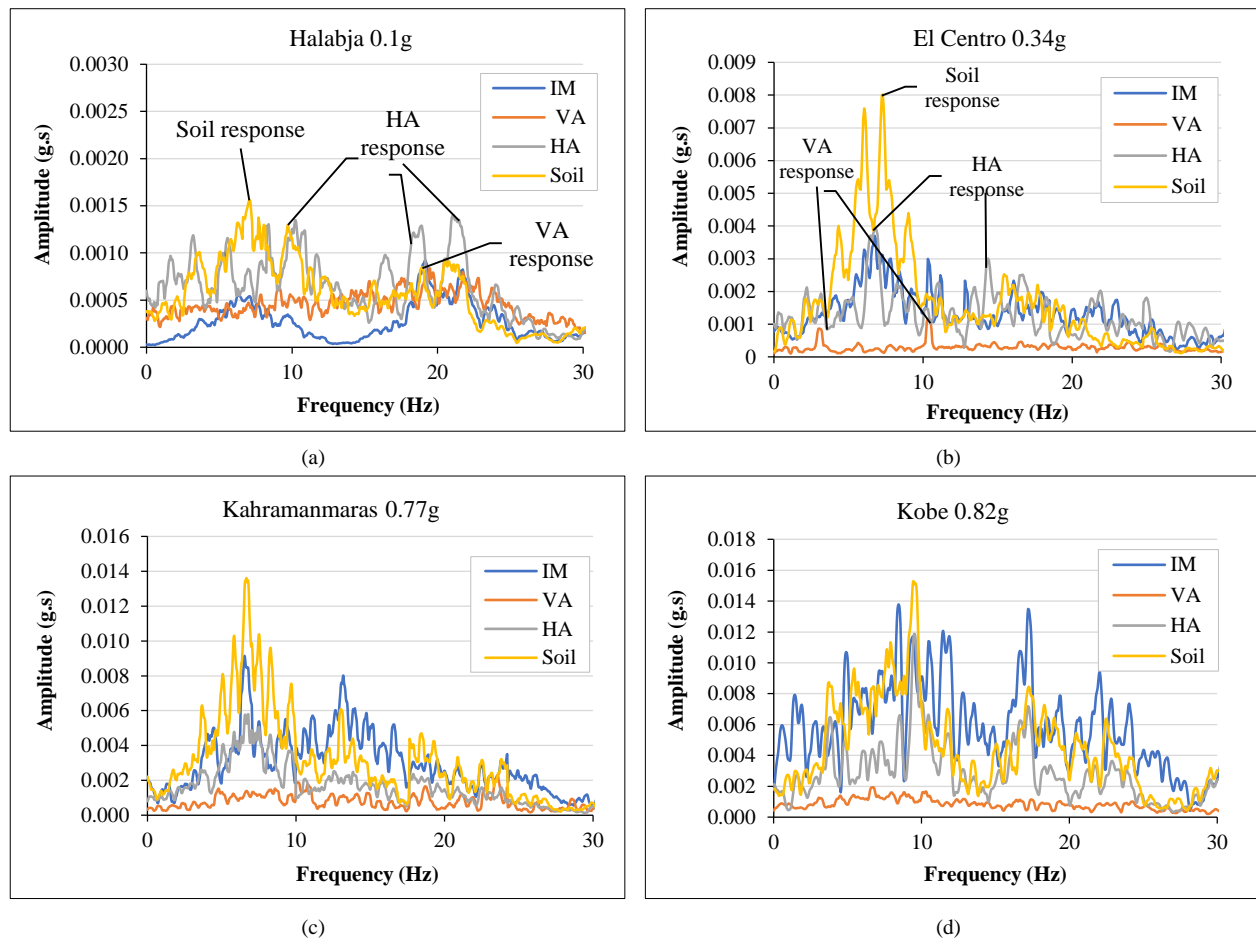


Figure 20. Frequency contents of piled machine foundation (5D, 20Hz) under Various Intensities: (a) Halabja (0.1g), (b) El Centro (0.34g), (c) Kahramanmaras (0.77g), (d) Kobe (0.82g)

El Centro (0.34g): As illustrated in Figure 20-b, the soil exhibits resonance between 5-7 Hz, with the peak amplitude reaching twice that of the dominant input motion. The horizontal acceleration resonated prominently at 7 Hz, followed by diminishing peaks at higher frequencies. In contrast, vertical acceleration showed negligible effects, indicating no significant resonance in this component.

Kahramanmaras (0.77g): As shown in Figure 20-c, the soil resonates at 6-7 Hz, displaying an amplified response compared to the dominant frequency in the Fourier amplitude. The horizontal acceleration also resonates at this frequency, although with a slightly lower Fourier amplitude than the dominant frequency, whereas the vertical acceleration remains unaffected by significant resonance.

Kobe (0.82g): As depicted in Figure 20-d, the soil and horizontal acceleration demonstrate resonance at 9.3 Hz, with the soil response slightly below the dominant frequency in the Fourier amplitude. The vertical acceleration showed no significant effects, indicating that the primary dynamic response was concentrated in the soil and horizontal components.

As illustrated in Figure 21-a, during the Halabja earthquake (0.1 g) at an operating frequency of 30 Hz, resonance was observed within the soil and machine foundation system, particularly in the 6-8 Hz frequency range. The soil acceleration and the horizontal and vertical accelerations of the machine were amplified by factors of 4.5, 1.5, and 1, respectively, relative to the Fourier amplitude at the dominant frequency.

El Centro (0.34g): As depicted in Figure 21-b, resonance occurs in both the soil and horizontal acceleration at 6-7 Hz, with Fourier amplitudes reaching twice that of the dominant frequency. Vertical acceleration exhibits marginal resonance at the same frequency, with an amplification of less than twice the Fourier amplitude of the dominant frequency.

Kahramanmaras (0.77g): As shown in Figure 21-c, the soil resonates at 6-7 Hz, with amplification exceeding that of the dominant frequency. The horizontal acceleration also resonates at this frequency but with a lower Fourier amplitude than the dominant frequency. The vertical acceleration shows no significant resonance effect.

Kobe (0.82g): As illustrated in Figure 21-d, the soil exhibits resonance at two distinct peaks, 5 and 9 Hz, with Fourier amplitudes surpassing the dominant frequency. The horizontal acceleration exhibits peak at 5 Hz, 9.5 Hz, 17, and 22 Hz, with the highest amplification at 9.5 Hz. However, the vertical acceleration showed no significant resonance effect.

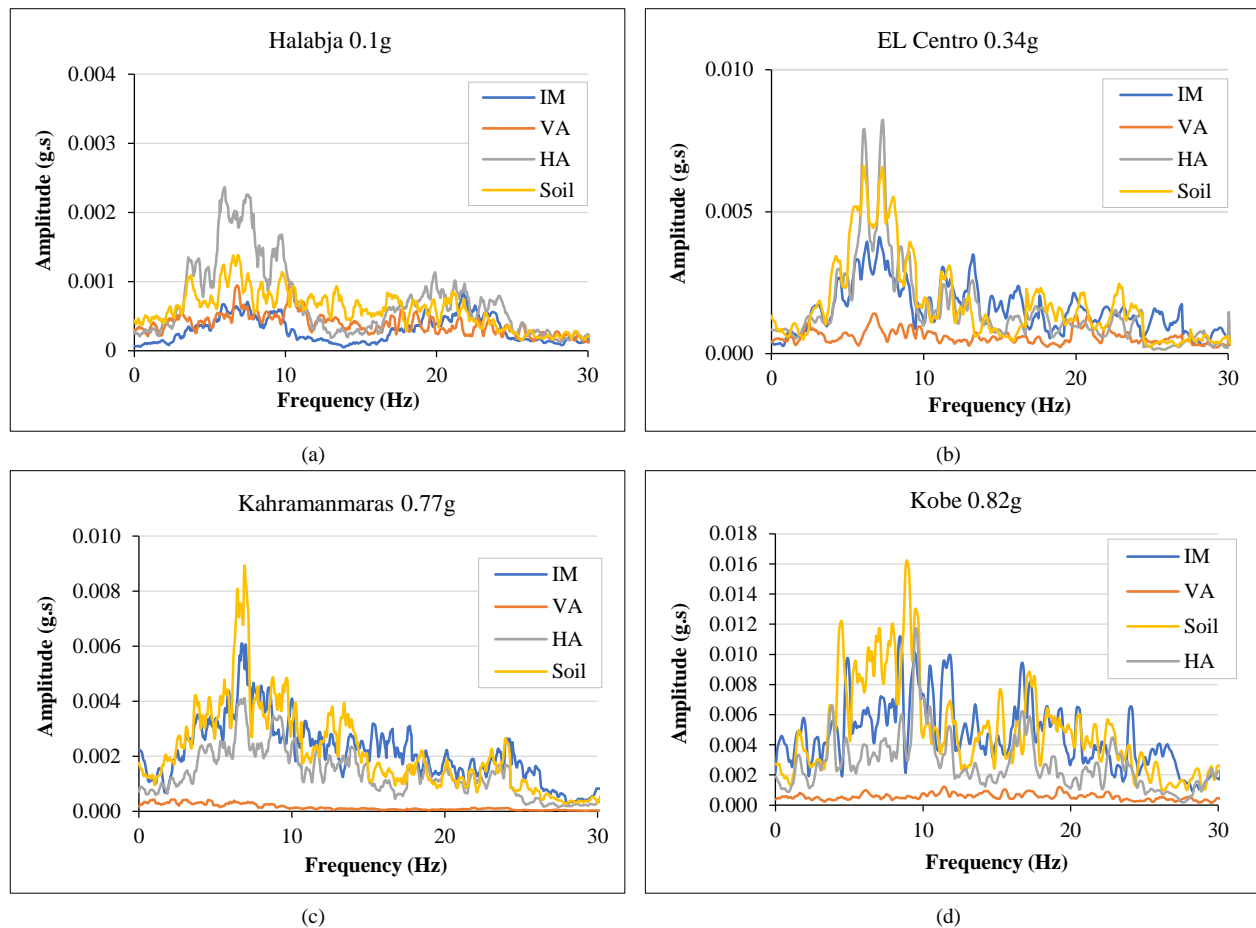


Figure 21. Frequency contents of piled machine foundation (SD, 30Hz) under Various Intensities: (a) Halabja (0.1g), (b) El Centro (0.34g), (c) Kahramanmaras (0.77g), (d) Kobe (0.82g)

This phenomenon can be attributed to non-stationary frequency effects, as detailed in previous studies [96-98] which was evident in test results. The non-stationary frequency refers to the variation in dominant seismic frequencies across different phases, resulting in each frequency component reaching its peak at different times. The dynamic response and resonance behaviour of the piled machine foundation system are notably more pronounced at lower frequencies and seismic intensities. At low intensities, such as 0.1 g, the soil and horizontal accelerations exhibit significant amplification owing to the elastic behaviour of the soil, resulting in peak acceleration values consistent with the previous discussions. Conversely, vertical acceleration showed less sensitivity to higher intensities, whereas soil and horizontal accelerations increased with greater seismic intensities.

Examination of the dynamic response of the piled machine foundation revealed the following key observations:

- **Harmonic Resonance:** The peaks of the vertical acceleration indicate the occurrence of harmonic resonance, where vertical vibrations interact with vertically propagating waves induced by horizontal motion, resulting in complex dynamic responses [41, 95].
- **Higher Mode Effects:** The multiple peaks in the HA indicate the occurrence of higher mode effects, where different frequencies excite various vibrational modes of the foundation system, which impact the dynamic response [99].
- **Nonlinear Behaviour:** The varying resonance and amplification patterns across different frequencies and earthquake intensities may be due to the nonlinear behaviour of the soil and foundation system, which is influenced by the soil-structure interaction and higher harmonic components [87, 100-102].
- **Rotating machinery with eccentric masses** can induce gyroscopic and circulatory forces that significantly influence system stability. Gyroscopic forces, generated by the angular momentum of the rotating components, can stabilize the system by counteracting destabilizing influences, similar to how a spinning top maintains balance. Circulatory forces, which arise from the interaction between the rotating parts and surrounding medium, further contribute to this dynamic behaviour. In piled machine foundations, these forces help mitigate excessive horizontal accelerations under harmonic and seismic loads, thereby ensuring the stability of the foundation and supported structure. Different circumstances under which these types of forces may arise have been reported in the literature [103]. Gyroscopic and circulatory forces are represented by skew-symmetric components of the damping and stiffness matrices of rotating machinery structures, respectively [104-105].

To address how harmonic resonance was identified in the experimental data, I have elaborated on the following points:

1. Introduction to Resonance:

Resonance occurs when a system is subjected to a frequency that matches its natural frequency, leading to amplified oscillations. This phenomenon can be identified by observing significant increases in amplitude at specific frequencies.

2. Types of Motion:

- Simple Harmonic Motion (SHM): Characterized by repetitive oscillatory movement at consistent intervals, described by trigonometric functions.
- Subharmonic Motion: Frequencies that are fractions of the fundamental excitation frequency, often observed in nonlinear systems.
- Superharmonic Motion: Frequencies that are integer multiples of the fundamental frequency, occurring in systems with nonlinearities (Figure 22).

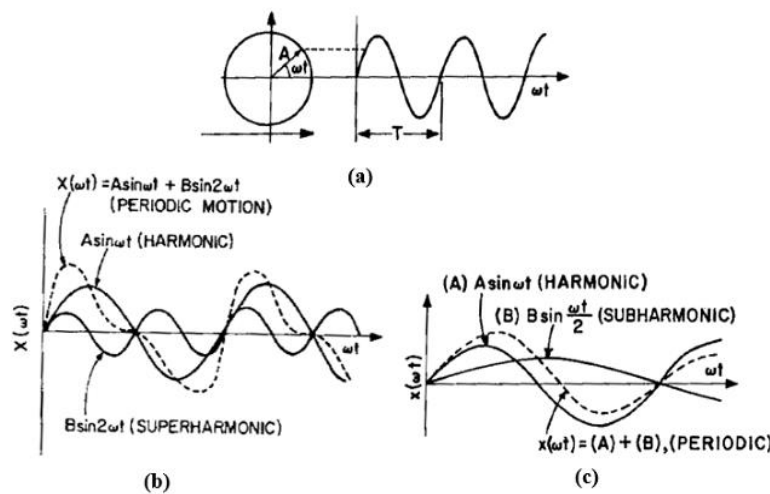


Figure 22. (a) Harmonic motion $A \sin \omega t$ and its vector representation, (b) Subharmonic, harmonic, and periodic motions, (c) Superharmonic, harmonic, and periodic motions [41]

3. Detection in Experimental Data:

- Three-Axis Acceleration Measurement: To capture comprehensive data on vibrations, accelerometers were placed along three axes. The vertical axis showed the highest amplitude acceleration, indicating significant vertical vibration, as shown in Figure 23.

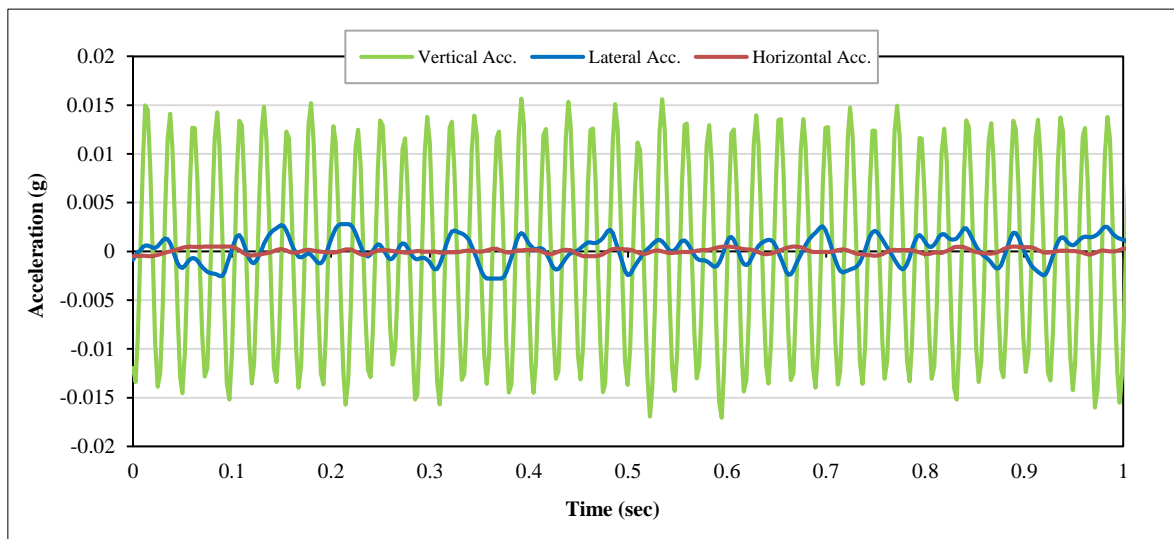


Figure 23. Comparative Analysis of Measured Acceleration Components at three axes

- Frequency Analysis: Fast Fourier Transform (FFT) was used to analyze frequency components. Resonance was identified by observing amplification at specific frequencies corresponding to the system’s natural frequencies. If multiple curves in the FFT analysis coincide, it suggests that resonance is occurring.

3.4. Spectral Acceleration Analysis (Sa)

Spectral acceleration analysis was employed to investigate the dynamic responses across different frequencies. Figure 24-a illustrates the spectral response of the Halabja earthquake at 10 Hz. The input motion exhibits two peaks: a primary peak at 0.06 seconds (0.28 g) and a secondary peak at 0.12 seconds (0.24 g). The soil response demonstrates significant resonance with peaks at 0.04 seconds (0.36 g) and 0.16 seconds (0.36 g). The horizontal acceleration (HA) reaches two notable peaks: the primary at 0.06 seconds (0.57 g) and a secondary peak at 0.14 seconds (0.44 g), with a smaller peak at 0.30 seconds (0.25 g), indicating substantial amplification. The vertical acceleration (VA) is highest at 0.06 seconds (0.10 g).

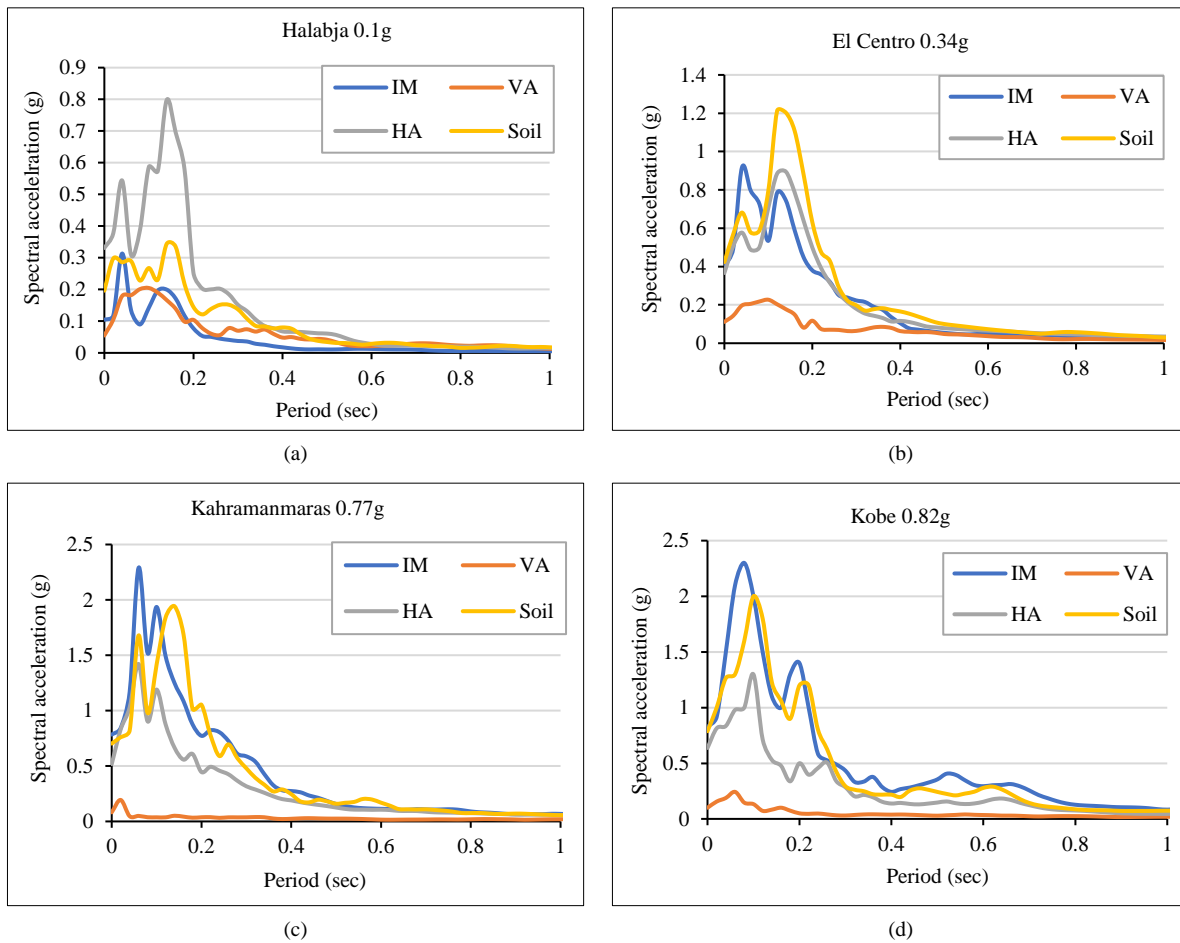


Figure 24. Spectral acceleration of piled machine foundation ($\zeta=5\%$, 5D, 10Hz) under Various Intensities: (a) Halabja (0.1g), (b) El Centro (0.34g), (c) Kahramanmaraş (0.77g), (d) Kobe (0.82g)

In the El Centro earthquake, as shown in Figure 24-b, the input motion peaks at 0.06 seconds (0.85 g) and 0.16 seconds (0.68 g). The soil response peaks at 0.06 seconds (0.74 g), reflecting significant resonance. The horizontal acceleration (HA) exhibits two peaks: the primary at 0.04 seconds (1.17 g) and a secondary peak at 0.14 seconds (0.74 g), indicating substantial amplification. The vertical acceleration (VA) peaks at 0.02 seconds with 0.29 g.

Figure 24-c depicts the Kahramanmaraş earthquake response, showing intensity measures (IM) with peaks at 0.08 seconds (2.3 g) and 0.12 seconds (1.84 g). The soil response peaks at 0.06 seconds (1.5 g) and 0.14 seconds (1.95 g), indicating significant soil resonance. The horizontal acceleration (HA) exhibits peaks at 0.08 seconds (0.97 g) and 0.14 seconds (1.18 g), reflecting substantial amplification compared to the input motion. The vertical acceleration (VA) peaks at 0.12 seconds with 0.22 g.

In Figure 24-d for the Kobe earthquake, the input motion shows initial peaks at 0.06 seconds (2.5 g) and 0.14 seconds (2 g). The soil response exhibits peak at 0.06 seconds (1.74 g) and 0.14 seconds (2 g), indicating significant resonance. The horizontal acceleration (HA) has primary peaks at 0.10 seconds (1.5 g) and another 0.22 seconds (0.6 g), resulting

from considerable amplification. The vertical acceleration (VA) peaks at 0.06 seconds (0.22 g) and 0.12 seconds (0.26 g), show some damping effects.

Figure 25-a illustrates the spectral acceleration characteristics of the Halabja earthquake at 20 Hz. The input motion peaks at 0.06 seconds (0.28 g) and 0.12 seconds (0.24 g). The soil response shows resonance with peaks at 0.04 seconds (0.36 g) and 0.16 seconds (0.36 g). The horizontal acceleration (HA) reaches its maximum at 0.06 seconds with 0.47 g, indicating amplification effects. The vertical acceleration (VA) peaks at 0.08 seconds with 0.21 g, reflecting the presence of damping. Figure 25-b shows the response of the El Centro earthquake. The input motion peaks at 0.06 seconds (0.85 g) and 0.16 seconds (0.68 g). The soil response peaks at 0.06 seconds with 0.74 g, indicating some amplification, but remains slightly lower than the input motion. The horizontal acceleration (HA) peaks at 0.08 seconds with 0.56 g. The vertical acceleration (VA) shows peaks at 0.10 seconds (0.26 g) and 0.20 seconds (0.16 g), demonstrating the effects of both amplification and damping. For the Kahramanmaraş earthquake, Figure 25-c reveals intensity measures (IM) with peaks at 0.08 seconds (2.3 g) and 0.12 seconds (1.84 g). The soil acceleration response exhibited peaks at 0.06 seconds (1.5 g) and 0.14 seconds (1.95 g), suggesting resonance. The horizontal acceleration (HA) shows peaks at 0.08 seconds (1.084 g), 0.12 seconds (1 g), and 0.20 seconds (0.62 g). The vertical acceleration (VA) reaches its highest value at 0.12 seconds with 0.22 g, indicating minimal amplification.

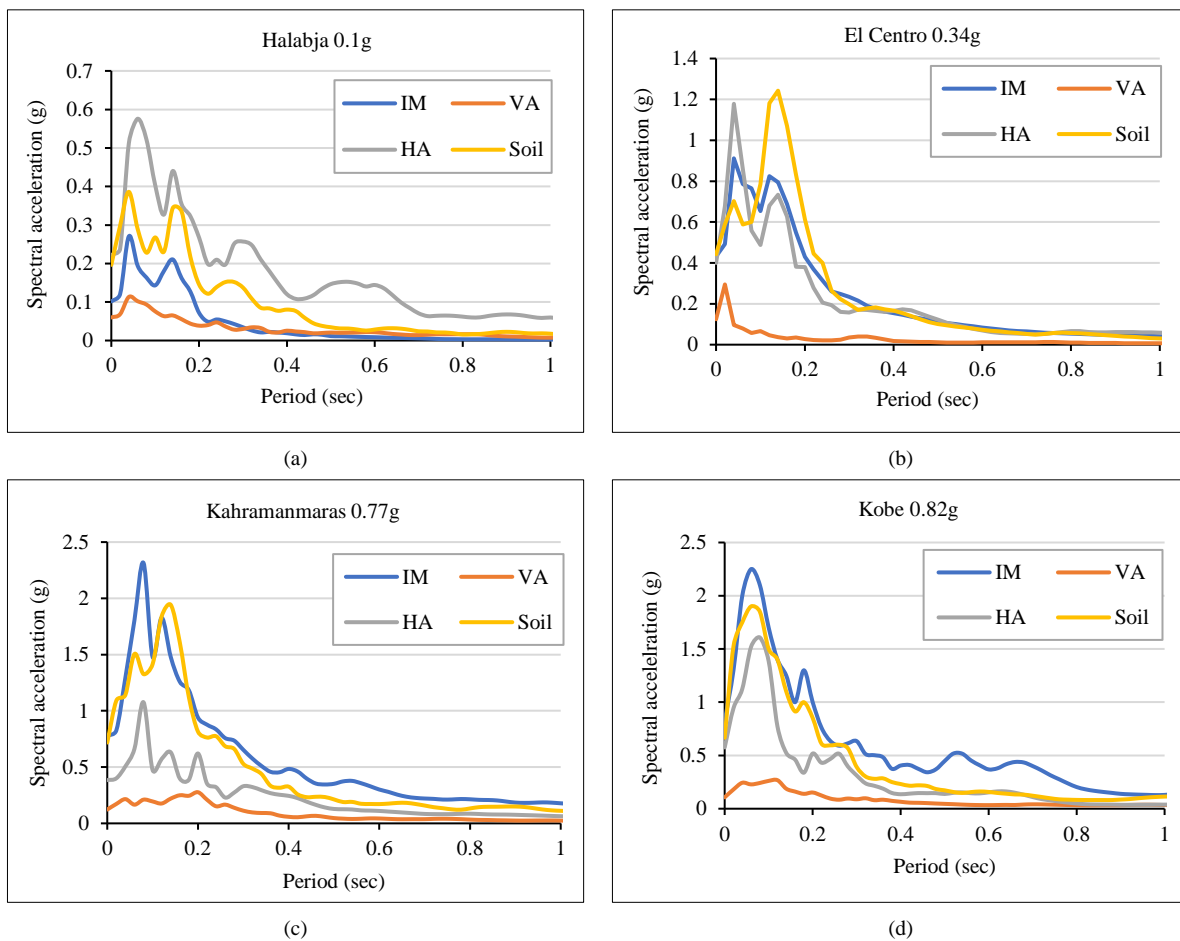


Figure 25. Spectral acceleration of piled machine foundation ($\zeta=5\%$,5D, 20Hz) under Various Intensities: (a) Halabja (0.1g), (b) El Centro (0.34g), (c) Kahramanmaraş (0.77g), (d) Kobe (0.82g)

Figure 25-d for the Kobe earthquake displays two peaks at 0.06 seconds (2.5 g) and 0.14 seconds (2 g). The soil response also shows peaks at 0.06 seconds (1.74 g) and 0.14 seconds (2 g), indicating significant soil resonance. The horizontal acceleration (HA) reaches primary peaks at 0.02 seconds (0.84 g) and 0.12 seconds (1 g), resulting from amplification. The vertical acceleration (VA) peaks at 0.14 seconds with 0.26 g, which is lower than the peak intensity measures.

Figure 26-a illustrates the spectral response of the Halabja earthquake at 30 Hz. The input motion exhibits two peaks: a primary peak at 0.06 seconds (0.28 g) and a secondary peak at 0.12 seconds (0.24 g). The soil response demonstrates significant resonance with peaks at 0.04 seconds (0.36 g) and 0.16 seconds (0.36 g). The horizontal acceleration (HA) reaches two notable peaks: the primary at 0.06 seconds (0.57 g) and a secondary peak at 0.14 seconds (0.44 g), with a smaller peak at 0.30 seconds (0.25 g), indicating substantial amplification. The vertical acceleration (VA) is highest at 0.06 seconds (0.10 g). In the El Centro earthquake, as shown in Figure 26-b, the input motion peaks at 0.06 seconds

(0.85 g) and 0.16 seconds (0.68 g). The soil response peaks at 0.06 seconds (0.74 g), reflecting significant resonance. The horizontal acceleration (HA) exhibits two peaks: the primary at 0.04 seconds (1.17 g) and a secondary peak at 0.14 seconds (0.74 g), indicating substantial amplification. The vertical acceleration (VA) peaks at 0.02 seconds with 0.29 g. Figure 26-c depicts the Kahramanmaraş earthquake response, showing intensity measures (IM) with peaks at 0.08 seconds (2.3 g) and 0.12 seconds (1.84 g). The soil response peaks at 0.06 seconds (1.5 g) and 0.14 seconds (1.95 g), indicating significant soil resonance. The horizontal acceleration (HA) exhibits peaks at 0.08 seconds (0.97 g) and 0.14 seconds (1.18 g), reflecting substantial amplification compared to the input motion. The vertical acceleration (VA) peaks at 0.12 seconds with 0.22 g. In Figure 26-d for the Kobe earthquake, the input motion shows initial peaks at 0.06 seconds (2.5 g) and 0.14 seconds (2 g). The soil response exhibits peak at 0.06 seconds (1.74 g) and 0.14 seconds (2 g), indicating significant resonance. The horizontal acceleration (HA) has primary peaks at 0.10 seconds (1.5 g) and another 0.22 seconds (0.6 g), resulting from considerable amplification. The vertical acceleration (VA) peaks at 0.06 seconds (0.22 g) and 0.12 seconds (0.26 g), show some damping effects.

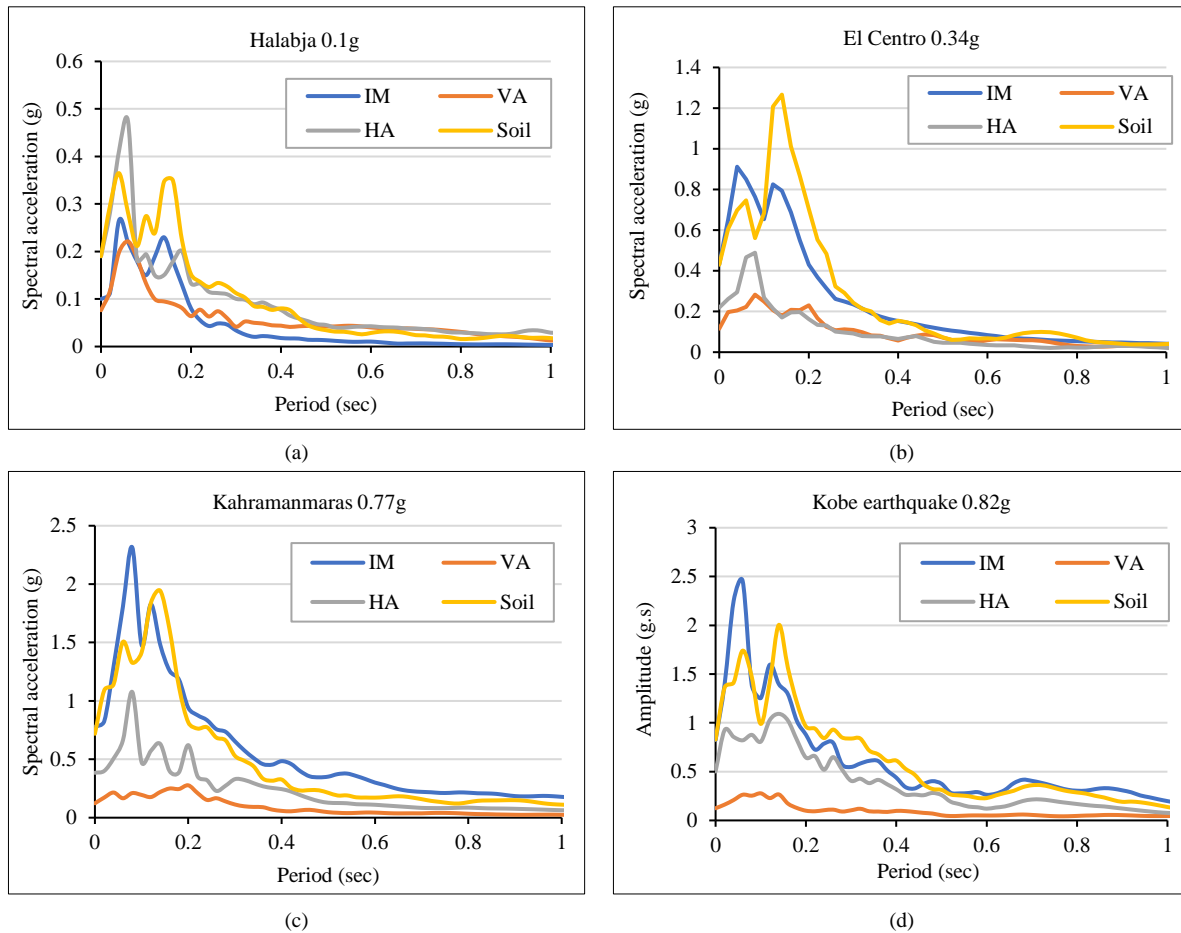


Figure 26. Spectral acceleration of piled machine foundation ($\zeta=5\%$, 5D, 30Hz) under Various Intensities: (a) Halabja (0.1g), (b) El Centro (0.34g), (c) Kahramanmaraş (0.77g), (d) Kobe (0.82g)

Figure 26-a illustrates the results of the Halabja earthquake. The soil response exhibits a peak period of approximately 0.1 seconds, indicating resonance and amplification of seismic waves up to 0.35 g, exceeding the input motion. The horizontal acceleration demonstrated multiple peaks, with the maximum occurring just beyond 0.1 seconds, reaching approximately 0.45 g. Which is attributed to significant resonance effects and higher-mode interactions within the foundation system. In contrast, the vertical acceleration presents a comparatively weak response, with an initial peak of around 0.07 seconds and a spectral acceleration of about 0.25 g. The soil response exhibits a peak period of approximately 0.1 seconds, indicating resonance and amplification of seismic waves up to 0.35 g, exceeding the input motion. The horizontal acceleration demonstrated multiple peaks, with the maximum occurring just beyond 0.1 seconds, reaching approximately 0.45 g due to resonance effects and higher-mode interactions within the foundation system. In contrast, the vertical acceleration presents a comparatively weak response, with an initial peak of around 0.07 seconds and a spectral acceleration of about 0.25 g, indicating effective damping and reduced resonance in the vertical direction at this intensity.

Figure 26-b illustrates the spectral acceleration analysis for the El Centro Earthquake. The soil exhibits a peak spectral acceleration at approximately 0.14 seconds, reaching 1.26 g, indicating resonance effects. The horizontal acceleration (HA) peaks at 0.08 seconds with a spectral acceleration of 0.48 g, while the input motion shows multiple peaks at 0.06

seconds (0.84 g) and 0.14 seconds (0.79 g). The vertical acceleration (VA) shows peaks at 0.10 seconds (0.26 g) and 0.16 seconds (0.20 g), suggesting effective damping. Figure 26-c shows the results of the Kahramanmaras earthquake. Intensity measures (IM) exhibited peaks at 0.08 seconds (2.31 g) and 0.12 seconds (1.84 g). The horizontal acceleration (HA) peaks at 0.08 seconds with 1.07 g, while the soil response peaks at 0.14 seconds with 1.94 g. The vertical acceleration (VA) peaks at 0.20 seconds with 0.27 g. Figure 26-d shows the spectral acceleration characteristics of the Kobe Earthquake. Intensity measures (IM) peak at 0.06 seconds (1.45 g). The soil response peaks at 0.14 seconds with 2.0 g, and the horizontal acceleration (HA) peaks at 0.12 seconds with 1.41 g. The vertical acceleration (VA) peaks at 0.14 seconds with 0.26 g

Figure 27 illustrates the observed response variations as a function of changes in the machine operating frequency and intensity of the historical earthquake input. A detailed analysis of these relationships is presented below:

Changing in machine operating frequency (10, 20, 30 Hz) as shown in Figure 27:

- *Soil Resonance:* At all frequencies (10, 20, and 30 Hz), the soil showed an amplification relative to the input motion (IM), particularly at lower intensities. The soil response was highest at all frequency with a 1.29 times amplification at 0.1 g and 0.34 g intensities, and it generally decreased as the intensity increased at 0.77 g and 0.82 g. The soil resonates at lower seismic intensities owing to nonlinear soil behavior. The same trend was observed by Kaynia [79] that the higher amplification factor can occur due to the interference within the group pile.
- *Horizontal Acceleration (HA):* The HA shows amplification across all frequencies, especially at 10 Hz, where it reaches 2.8 times the input motion at a density of 0.1 g due to the fact that increasing the frequency increases the vertical dynamic force induced by the rotating machine, as the amplification decreases with increasing frequency.
- *Vertical Acceleration (VA):* Generally, shows less amplification than soil acceleration and horizontal acceleration. At higher frequencies (30 Hz), VA showed the least amplification, which decreased with increasing frequency owing that the effective damping is in the vertical direction across all intensities.

2. Changing in input motion (earthquake) Intensities as shown in Figure 27:

- *Low Intensity (0.1g):* Both soil and HA spectral acceleration results showed significant amplification, with HA showing the highest amplification at 10 Hz (2 times IM). Observations show that low-intensity seismic waves can induce strong resonance in the HA region, particularly at low frequencies. It can be explained that the soil exhibits elastic behavior leading to high amplification of acceleration values as reported by Hussein & Naggar [50], that the soil behave linear till 0.1 g, whereas it exhibits nonlinear at 0.3 g and above.
- *Moderate Intensity (0.34g):* In the case of moderate intensity, the results showed that the amplification of soil and HA was significant, but less than that of low intensity. The vertical acceleration appears to show minimal resonance effects. The behavior can be explained by the soil and horizontal acceleration, which exhibit a stronger response at low intensity than at moderate acceleration. In addition, the soil behaves nonlinearly in this range, as discussed by Hussein & Naggar [50].
- *High Intensity (0.77g and 0.82g):* At high intensities, both soil and HA showed a marginal increase in amplification, but the amplification was less than that at low intensities [52]. IM becomes the dominant factor in amplification at high frequencies (30 Hz). VA showed minimal amplification, indicating effective damping mechanisms in the vertical direction, even during high-intensity seismic events.

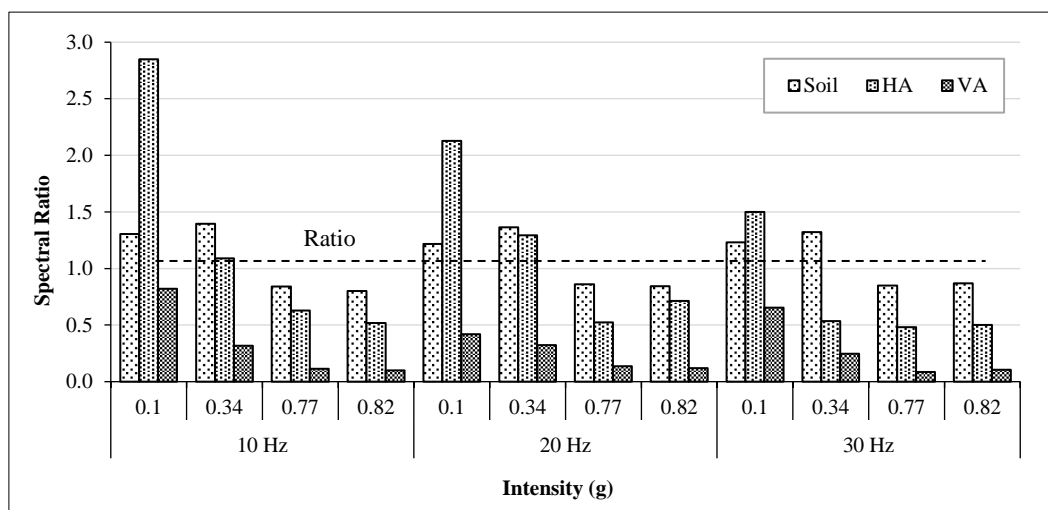


Figure 27. Seismic spectral ratio comparison across different frequencies and intensities

3.5. Acceleration Variation with Depth

Figure 28 to 35 illustrate the variation in acceleration with depth for both near-field (kinematic effects) and far-field (inertia of soil) conditions across different frequencies (0 Hz, 10 Hz, 20 Hz, and 30 Hz). This section specifically examines depths of $D/H=0.3$ and $D/H=0.5$, corresponding to 30 cm and 50 cm from the top surface of the machine, which equate to 10 cm and 30 cm below the soil surface, respectively (see Figure 28). The analysis aimed to elucidate the acceleration behavior near and far from the vibration source, highlighting the phase differences between the inertial and kinematic effects.

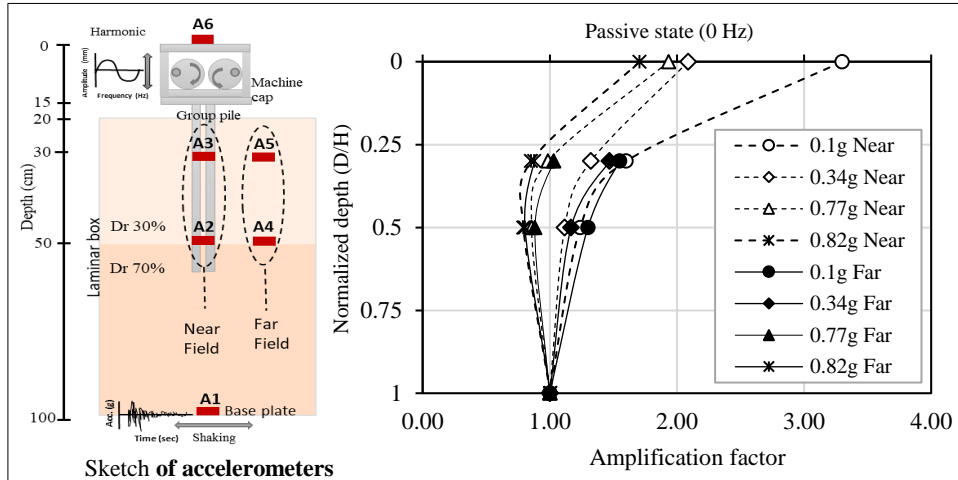


Figure 28. Amplification factor vs. normalized depth for near and far field at different intensities under passive state (0Hz)

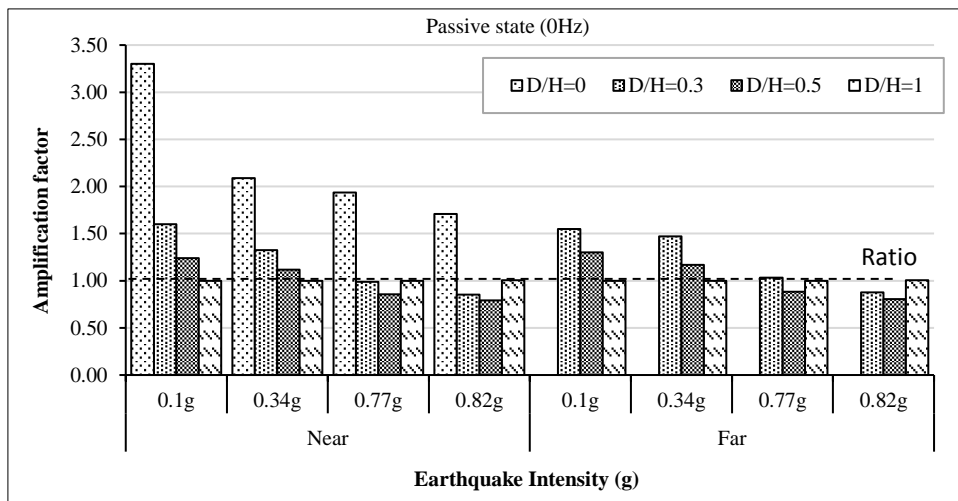


Figure 29. Amplification factor variation with earthquake intensity under passive state (0Hz)

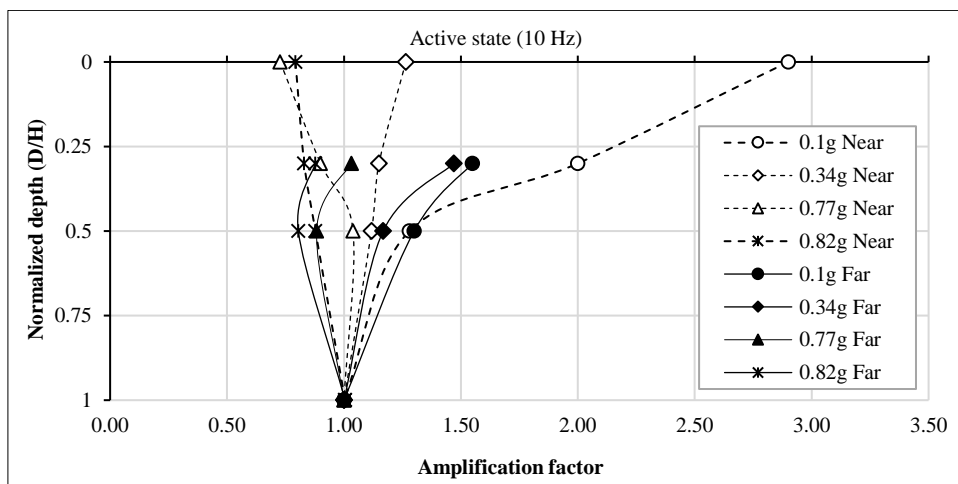


Figure 30. Amplification factor vs. normalized depth for near and far field at different earthquake intensity under operating frequency of (10Hz)

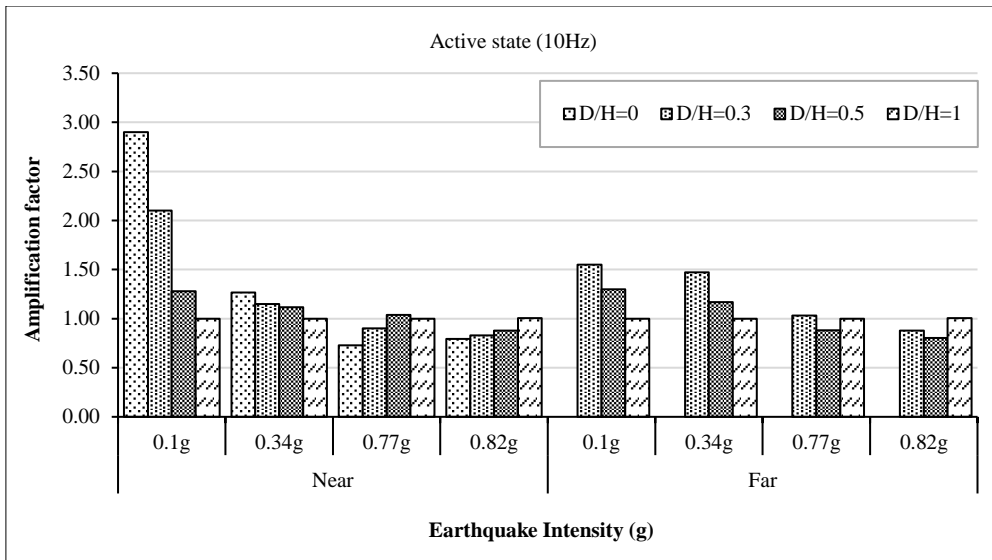


Figure 31. Amplification factor variation with earthquake intensity at operating frequency of (10Hz)

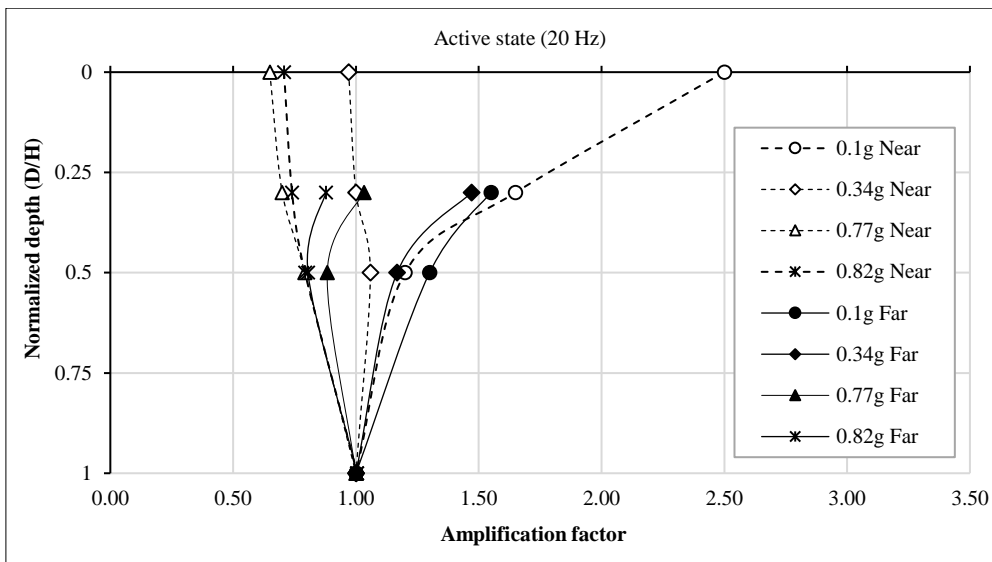


Figure 32. Amplification factor vs. normalized depth for near and far field at different earthquake intensity under operating frequency of (20Hz)

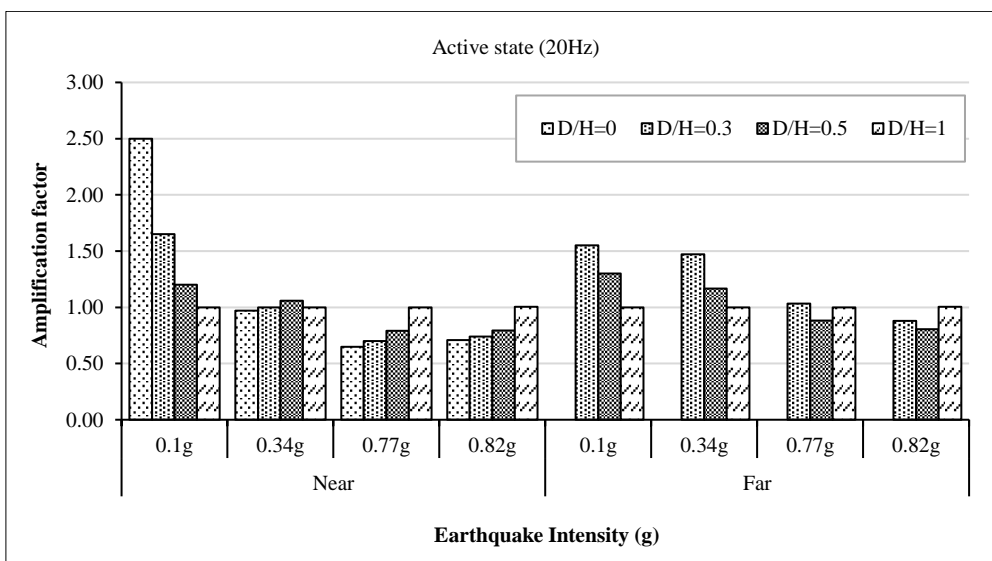


Figure 33. Amplification factor variation with earthquake intensity at operating frequency of (20Hz)

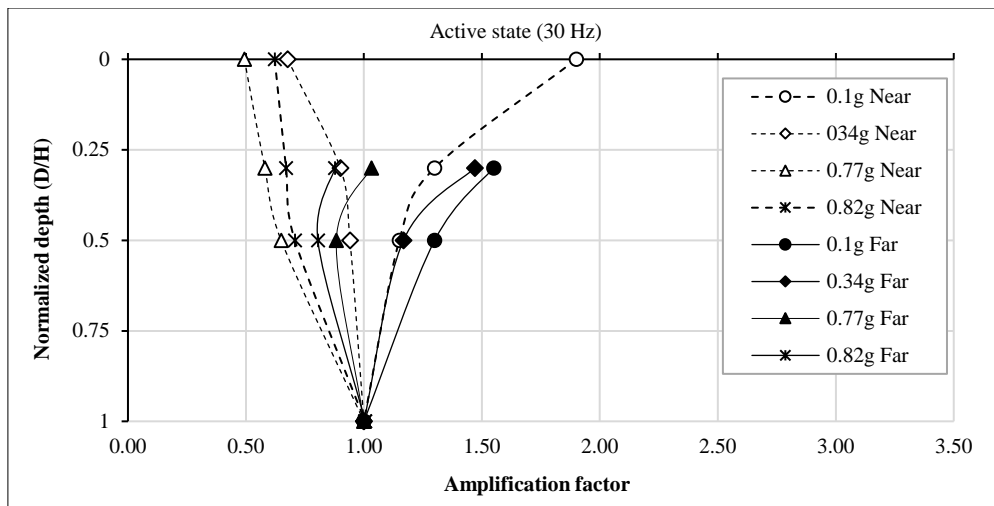


Figure 34. Amplification factor vs. normalized depth for near and far field at different earthquake intensity under operating frequency of (30Hz)

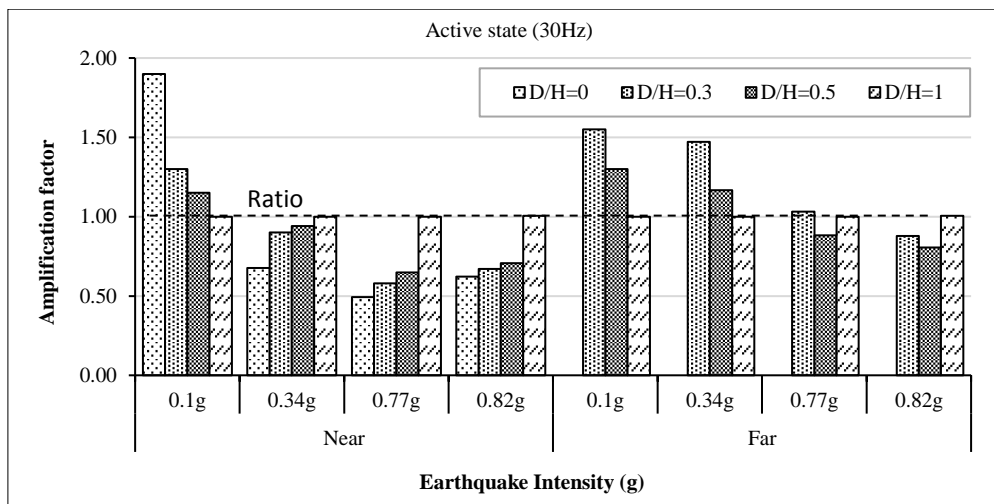


Figure 35. Amplification factor vs. normalized depth for near and far field at operating frequency of (30Hz)

3.5.1. Passive State (0 Hz)

Figures 28 and 29 present the acceleration profiles at 0 Hz, highlighting the distinct inertial and kinematic phase differences observed at depths of $D/H = 0.3$ and $D/H = 0.5$ under various earthquake intensities. At an intensity of 0.1 g, the near field exhibits a 3% reduction in acceleration compared to the far field. However, as the earthquake intensity increases to 0.34 g, 0.77 g, and 0.82 g, the near field acceleration decreases by 11%, 5%, and 3%, respectively, relative to the far field. This trend indicates that the discrepancy in acceleration between the near and far fields diminished as the earthquake intensity increased.

3.5.2. Active State (10 Hz)

Figures 30 and 31 show the acceleration profiles at 10 Hz. At a depth of $D/H = 0.3$, the near-field acceleration consistently registers lower values than the far-field acceleration. For instance, at an intensity of 0.1 g, the near-field acceleration is reduced by 16% relative to the far field. This trend becomes more pronounced with increasing earthquake intensities, particularly at 0.77 g. The observed attenuation is attributed to the interference between machine vibrations and seismic waves, as discussed by Gazetas [86]. This interference effect amplifies the difference in the acceleration between the near and far fields.

3.5.3. Active State (20 Hz)

Figures 32 and 33 show the acceleration profiles at 20 Hz, respectively. Consistent with the observations at 10 Hz, the near-field acceleration was generally lower than that of the far field. Specifically, at an intensity of 0.34 g, the near-field acceleration is reduced by 47% compared to the far field. This attenuation effect became more pronounced at higher intensities, reflecting a significant interaction between machine-induced vibrations and seismic waves.

3.5.4. Active State (30 Hz)

Figures 34 and 35 show the acceleration profiles at 30 Hz. The near-field acceleration remained lower than that in the far-field. At an intensity of 0.34 g, the near field shows a 28% reduction in acceleration compared to the far field. The attenuation effect is less pronounced than that at 20 Hz.

Figure 36 details the percentage differences in amplification factors between the far-field and near-field conditions across various earthquake intensities and frequencies. The figure highlights the extent to which the inertial response of the soil layer surpasses the kinematic response of the piled system, a trend also observed by Garala & Madabhushi [52]. Normalized depths (D/H) of 0.3 and 0.5 were used to analyze changes in the amplification factor at different depths. The percentage difference was calculated using the following formula.

$$PD = \frac{A_{far} - A_{near}}{A_{near}} \times 100 \quad (9)$$

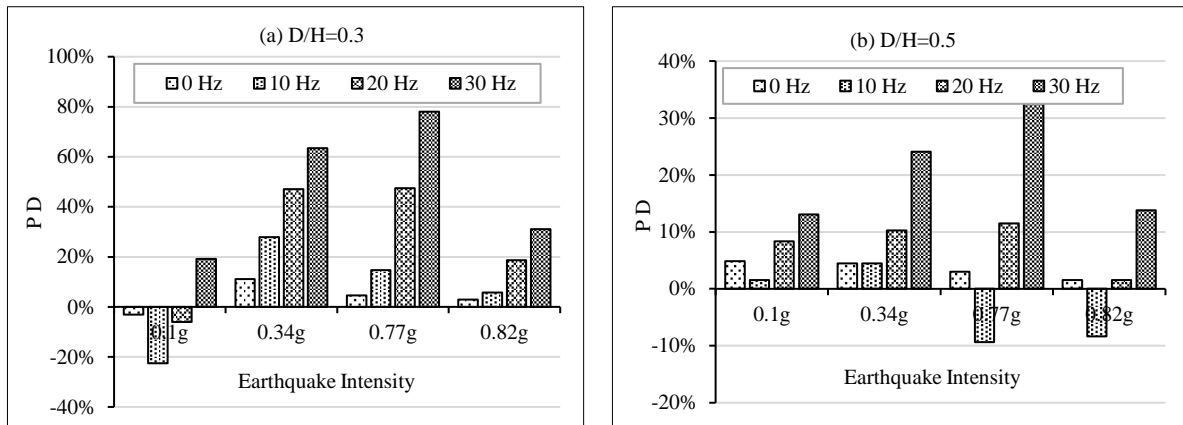


Figure 36. percentage difference in acceleration between far field and near field across various frequencies and earthquake intensities, (a) D/H=0.3, (b) D/H =0.5

The observations of acceleration in both the far and near fields, as depicted in Figure 33, reveal the following key points:

- **Inertial vs. Kinematic Responses:** The near field generally exhibits less acceleration compared to the far field, indicating that the inertial response of the soil layer is greater than the kinematic response of the piled system. This phase difference, as discussed by Garala & Madabhushi [52], tends to increase at higher frequencies, reaching a maximum value at 10 Hz at D/H = 0.3.
- **At D/H=0.3,** the trend line indicates that at shallower depths, there was a noticeable reduction in the horizontal acceleration values across different earthquake intensities and frequencies. This could be attributed to several factors:
 1. Interference and Harmonics: Seismic waves interacting with harmonic waves induced by the machine within the pile group.
 2. Resonance Effects: Under low frequencies especially at (10Hz), resonance effects might cause attenuation of acceleration due to wave interference.
 3. Inertial and Kinematic Effects: The configuration of the piled machine foundation (elevated cap, foundation mass and height) can affect on the propagation and absorption or transmission of seismic energy in the system.
 4. Nonlinear Soil Behavior: Nonlinear soil behavior can affect the way waves propagate and affect the appearance of acceleration values at varying depths.
 5. The far field in general trend shows acceleration values more than the near field, which indicates that it is less affected by harmonic waves induced by the machine compared to the near field.
- **At D/H=0.5,** at deeper depths, the convergence of the acceleration values indicates a significant response to seismic events. The influencing factors can be listed as follows [88, 92, 94, 106]:
 1. *Mitigating Surface Effects:* Deeper depths can mitigate seismic waves through shallower depths, which can amplify or attenuate.
 2. *Propagation dynamics:* Seismic waves can propagate differently at different depths, which affects acceleration values.
 3. *Reflection of wave and absorption:* Interaction between incoming seismic waves and the foundation system effects on the energy is reflected or absorbed within the group piles.

4. Conclusions

This study advances our understanding of the impact of vertical vibrations on the dynamic response of pile groups embedded in sandy soil under seismic loading conditions. Using an experimental setup with a piled machine foundation subjected to vertical vibrations at frequencies of 10, 20, and 30 Hz, and sequentially exposed to varying seismic accelerations, the following conclusions were drawn:

- Mitigation efficiency: The results showed a significant reduction in the horizontal acceleration, reaching 64% at 30 Hz. The mitigation efficiency increased with increasing PGA levels, showing decreases of 42, 68, 75, and 63% at PGA values of 0.1 g, 0.34 g, 0.77 g and 0.82 g, respectively. The damping system proved effective at high frequencies. Moreover, the damping efficiency at 30 Hz exceeded those at both 10 and 20 Hz.
- The Horizontal Amplification Factor (HAF) shows a large amplification that depends on the frequency. The HAF decreases from 2.9 times to 1.9 times as the frequency increased from 10 Hz to 30 Hz for the lowest seismic intensity of 0.1 g. The HAF increased by 43%, 47%, 32% and 22% for input shaking accelerations of 0.1g, 0.34g, 0.77g and 0.82g respectively when frequency increased from 10Hz to 30Hz.
- The VAF decreased with increasing frequency. The VAF decreased from 32% to 5% with an increase in frequency from 10 Hz to 30 Hz, indicating that low frequencies can be significantly affected by earthquakes.
- Harmonic Resonance: Peaks in vertical acceleration indicate the occurrence of harmonic resonance, where vertical vibrations interact with vertically propagating waves induced by horizontal motion.
- The elastic behavior of the soil at low intensities (0.1 g) may lead to the soil being amplified to the highest value at a low frequency of 10 Hz.
- Seismic excitation may amplify displacement amplitudes beyond the limit thresholds established by Blake (1964) and the ACI standards. Amplification was greater at lower frequencies and higher seismic intensity levels.
- Far-field accelerations exceed near-field accelerations, particularly in surface layers. This difference is attributed to the predominance of soil inertial movement over the kinematic response of the pile system. Contributing factors include interference effects, resonance phenomena, and nonlinear soil dynamics.
- Practical Implications for Earthquake Mitigation: This study supports the use of vertical vibrations as an effective method for reducing horizontal acceleration and enhancing seismic resilience. Vertical vibrations can be employed in various applications, such as pendulum-based damping systems in skyscrapers or spring-based base isolation tuned to low frequencies.
- However, caution is required when operating at frequencies below 10 Hz, as these lower frequencies may induce resonance and interact adversely with horizontal accelerations during earthquakes. Practical considerations should include designing systems to avoid these frequencies or implementing additional damping measures to mitigate the potential resonance effects.
- The displacement severity increases with decreasing frequency, peaking at 10 Hz, increasing the risk of faults owing to seismic wave interference. Maintaining displacement limits is critical for preventing structural and operational failures of machine components. Rigorous design and maintenance protocols are essential for ensuring resilience during seismic events.

5. Declarations

5.1. Author Contributions

Conceptualization, B.J.N. and B.S.A.; methodology, B.J.N.; validation, B.J.N. and B.S.A.; formal analysis, B.J.N.; investigation, B.J.N.; resources, B.J.N.; data curation, B.J.N.; writing—original draft preparation, B.J.N.; writing—review and editing, B.J.N. and B.S.A.; visualization, B.J.N.; supervision, B.S.A.; project administration, B.S.A.; funding acquisition, B.J.N. All authors have read and agreed to the published version of the manuscript.

5.2. Data Availability Statement

The data presented in this study are available on request from the corresponding author.

5.3. Funding

This research was supported by authors' personal resources. In addition, the University of Diyala provided partial funding and support for the construction of the shaking table used in the experiments.

5.4. Acknowledgements

The authors would like to express their gratitude to the University of Baghdad for their academic support, followed by the Ministry of Education - General Directorate of Education in Diyala Governorate for their assistance. Special thanks also go to the University of Diyala for their partial funding and support in constructing the shaking table used in this study. Additionally, we appreciate the assistance of all the colleagues and technical staff who contributed to this project.

5.5. Conflicts of Interest

The authors declare no conflict of interest.

6. References

- [1] Novak, M. (1974). Dynamic Stiffness and Damping of Piles. *Canadian Geotechnical Journal*, 11(4), 574–598. doi:10.1139/t74-059.
- [2] Novak, M. (1977). Vertical Vibration of Floating Piles. *ASCE Journal of the Engineering Mechanics Division*, 103(1), 153–168. doi:10.1061/jmcea3.0002201.
- [3] Novak, M., & El Sharnouby, B. (1983). Stiffness constants of single piles. *Journal of Geotechnical Engineering*, 109(7), 961–974. doi:10.1061/(ASCE)0733-9410(1983)109:7(961).
- [4] Novak, M., & Aboul-Ella, F. (1978). Impedance Functions of Piles in Layered Media. *Journal of the Engineering Mechanics Division*, 104(3), 643–661. doi:10.1061/jmcea3.0002366.
- [5] Novak, M., & Aboul-Ella, F. (1978). Stiffness and Damping of Piles in Layered Media. *Earthquake Engineering and Soil Dynamics-Proceedings of the ASCE Geotechnical Engineering Division Specialty Conference*, 19-21 June, 1978, Pasadena, United States.
- [6] Novak, M. & Sheta, M. (1980). Approximate approach to contact effects of piles. Special technical publication on dynamic response of pile foundations: Analytical aspects. *Proceedings of the Geotechnical Engineering Division, ASCE (1980)*, 53-79
- [7] Ei Naggar, M. H., & Novak, M. (1995). Effect of foundation nonlinearity on modal properties of offshore towers. *Journal of Geotechnical Engineering*, 121(9), 660–668. doi:10.1061/(asce)0733-9410(1995)121:9(660).
- [8] El Naggar, M. H., & Novak, M. (1996). Nonlinear analysis for dynamic lateral pile response. *Soil Dynamics and Earthquake Engineering*, 15(4), 233–244. doi:10.1016/0267-7261(95)00049-6.
- [9] Asgarian, B., Assareh, M. A., & Alanjari, P. (2008). Nonlinear Behavior of Single Piles in Jacket Type Offshore Platforms Using Incremental Dynamic Analysis. Volume 2: Structures, Safety and Reliability, 139–148. doi:10.1115/omae2008-57148.
- [10] Chau, K. T., & Yang, X. (2005). Nonlinear Interaction of Soil–Pile in Horizontal Vibration. *Journal of Engineering Mechanics*, 131(8), 847–858. doi:10.1061/(asce)0733-9399(2005)131:8(847).
- [11] Krishnan, R., Gazetas, G., & Velez, A. (1983). Static and dynamic lateral deflexion of piles in non-homogeneous soil stratum. *Geotechnique*, 33(3), 307–325. doi:10.1680/geot.1983.33.3.307.
- [12] Wu, G., & Finn, W. D. L. (1997). Dynamic elastic analysis of pile foundations using finite element method in the frequency domain. *Canadian Geotechnical Journal*, 34(1), 34–43. doi:10.1139/t96-87.
- [13] Kaynia, A. M. (1982). Dynamic stiffness and seismic response of pile groups. Ph.D. Thesis, Massachusetts Institute of technology, Cambridge, United States.
- [14] Banerjee, P. K., Sen, R., & Davies, T. G. (1987). Static and dynamic analyses of axially and laterally loaded piles and pile groups. Gulf Publishing Co, Houston, United States.
- [15] Ayothiraman, R., & Boominathan, A. (2006). Observed and Predicted Dynamic Lateral Response of Single Pile in Clay. *Soil and Rock Behavior and Modeling*, 367–374. doi:10.1061/40862(194)49.
- [16] Fattah, M. Y., Hamood, M. J., & Al-Naqdi, I. A. A. (2015). Finite-element analysis of a piled machine foundation. *Proceedings of the Institution of Civil Engineers: Structures and Buildings*, 168(6), 421–432. doi:10.1680/stbu.14.00053.
- [17] Fattah, M. Y., Hamood, M. J., & Al-Nakdy, I. A. M. (2020). Dynamic Response of Machine Foundation Resting on End Bearing Piles. *IOP Conference Series: Materials Science and Engineering*, 978(1), 12038. doi:10.1088/1757-899X/978/1/012038.
- [18] M. Al-Nakdy, I., Y. Fattah, M., & J. Hamood, M. (2014). Finite Element Analysis of Machine Foundation Resting on End Bearing Piles. *Engineering and Technology Journal*, 32(1A), 132–153. doi:10.30684/etj.32.1a.11.
- [19] Al-Jeznawi, D., Jais, I. B. M., & Albusoda, B. S. (2022). a Soil-Pile Response Under Coupled Static-Dynamic Loadings in Terms of Kinematic Interaction. *Civil and Environmental Engineering*, 18(1), 96–103. doi:10.2478/cee-2022-0010.

- [20] Al-Jeznawi, D., Mohamed Jais, I. B., Albusoda, B. S., & Khalid, N. (2022). Numerical modeling of single closed and open-ended pipe pile embedded in dry soil layers under coupled static and dynamic loadings. *Journal of the Mechanical Behavior of Materials*, 31(1), 587–594. doi:10.1515/jmbm-2022-0055.
- [21] Al-Jeznawi, D., Mohamed Jais, I. B., Albusoda, B. S., & Khalid, N. (2022). The slenderness ratio effect on the response of closed-end pipe piles in liquefied and non-liquefied soil layers under coupled static-seismic loading. *Journal of the Mechanical Behavior of Materials*, 31(1), 83–89. doi:10.1515/jmbm-2022-0009.
- [22] Fattah, M. Y., Zbar, B. S., & Mustafa, F. S. (2017). Vertical vibration capacity of a single pile in dry sand. *Marine Georesources & Geotechnology*, 35(8), 1111–1120. doi:10.1080/1064119X.2017.1294219.
- [23] Fattah, M. Y., Zbar, B. S., & Mustafa, F. S. (2021). Effect of soil saturation on load transfer in a pile excited by pure vertical vibration. *Proceedings of the Institution of Civil Engineers: Structures and Buildings*, 174(2), 132–144. doi:10.1680/jstbu.16.00206.
- [24] Fattah, M. Y., Zabar, B. S., & Mustafa, F. S. (2020). Effect of saturation on response of a single pile embedded in saturated sandy soil to vertical vibration. *European Journal of Environmental and Civil Engineering*, 24(3), 381–400. doi:10.1080/19648189.2017.1391126.
- [25] Choudhary, S. S., Biswas, S., & Manna, B. (2016). Dynamic coupled response of 6-pile groups with different pile arrangements. *Japanese Geotechnical Society Special Publication*, 2(38), 1389–1392. doi:10.3208/jgssp.ind-15.
- [26] Khandelwal, M., Bharathi, M., & Mukerjee, S. (2016). Behaviour of short pile under machine induced horizontal vibrations. *International Geotechnical Engineering Conference on Sustainability in Geotechnical Engineering Practices and Related Urban Issues*, 23-24 September, 2016, Mumbai, India.
- [27] Biswas, S., & Manna, B. (2018). Experimental and Theoretical Studies on the Nonlinear Characteristics of Soil-Pile Systems under Coupled Vibrations. *Journal of Geotechnical and Geoenvironmental Engineering*, 144(3), 4018007. doi:10.1061/(asce)gt.1943-5606.0001850.
- [28] Bhowmik, D., Baidya, D. K., & Dasgupta, S. P. (2013). A numerical and experimental study of hollow steel pile in layered soil subjected to lateral dynamic loading. *Soil Dynamics and Earthquake Engineering*, 53, 119–129. doi:10.1016/j.soildyn.2013.06.011.
- [29] Bhowmik, D., Baidya, D. K., & Dasgupta, S. P. (2016). A numerical and experimental study of hollow steel pile in layered soil subjected to vertical dynamic loading. *Soil Dynamics and Earthquake Engineering*, 85, 161–165. doi:10.1016/j.soildyn.2016.03.017.
- [30] Bharathi, M., Dubey, R. N., & Shukla, S. K. (2022). Dynamic response of underreamed batter piles subjected to vertical vibration. *International Journal of Geotechnical Engineering*, 16(8), 991–999. doi:10.1080/19386362.2021.2025304.
- [31] Choudhary, S. S., Biswas, S., & Manna, B. (2020). Experimental and numerical study of pile foundations subjected to rotating machine-induced coupled excitations. *International Journal of Geotechnical Engineering*, 14(6), 614–625. doi:10.1080/19386362.2019.1620536.
- [32] Choudhary, S. S., Biswas, S., & Manna, B. (2021). Effect of Pile Arrangements on the Dynamic Coupled Response of Pile Groups. *Geotechnical and Geological Engineering*, 39(3), 1963–1978. doi:10.1007/s10706-020-01599-6.
- [33] Sudhi, D., Sinha, S. K., Biswas, S., & Manna, B. (2023). Dynamic impedance parameters of floating piles subjected to coupled harmonic vibration. *Arabian Journal of Geosciences*, 16(9), 508. doi:10.1007/s12517-023-11615-7.
- [34] Dihoru, L., Bhattacharya, S., Taylor, C. A., Muir Wood, D., Moccia, F., Simonelli, A. L., & Mylonakis, G. (2009). Experimental modeling of kinematic bending moments of piles in layered soils. *Interface*, 1, 1-8.
- [35] Papazafeiropoulos, G., & Plevris, V. (2023). Kahramanmaraş—Gaziantep, Türkiye Mw 7.8 Earthquake on 6 February 2023: Strong Ground Motion and Building Response Estimations. *Buildings*, 13(5), 1194. doi:10.3390/buildings13051194.
- [36] Kavvads, M., & Gazetas, G. (1993). Kinematic seismic response and bending of free-head piles in layered soil. *Géotechnique*, 43(2), 207–222. doi:10.1680/geot.1993.43.2.207.
- [37] Mylonakis, G., Nikolaou, A., & Gazetas, G. (1997). Soil-pile-bridge seismic interaction: Kinematic and inertial effects. Part I: Soft soil. *Earthquake Engineering & Structural Dynamics*, 26(3), 337–359. doi:10.1002/(SICI)1096-9845(199703)26:3<337::AID-EQE646>3.0.CO;2-D.
- [38] Boulanger, R. W., Curras, C. J., Kutter, B. L., Wilson, D. W., & Abghari, A. (1999). Seismic Soil-Pile-Structure Interaction Experiments and Analyses. *Journal of Geotechnical and Geoenvironmental Engineering*, 125(9), 750–759. doi:10.1061/(asce)1090-0241(1999)125:9(750).
- [39] Youssef, A., Hegazy, M., & Mostafa, H. (2023). Performance of Isolated Footing with Several Corrosion Levels under Axial Loading. *Civil Engineering Journal*, 9(6), 1437-1455. doi:10.28991/CEJ-2023-09-06-011.
- [40] Liu, Z. (John). (2013). Design of Foundations for Large Dynamic Equipment in a High Seismic Region. *Structures Congress 2013*, 1403–1414. doi:10.1061/9780784412848.124.

- [41] Arya, S. C., O'Neill, M. W., & Pincus, G. (1979). Design of structures and foundations for vibrating machines. Gulf Publishing Company, Houston, United States.
- [42] Tripathy, S., & Desai, A. K. (2017). Analysis of seismically induced vibrations in turbo machinery foundation for different soil conditions: Case study. *Journal of Vibroengineering*, 19(6), 4356–4364. doi:10.21595/jve.2017.17436.
- [43] Noman, B. J., & Albusoda, B. S. (2023). Seismic Hazard Assessment in Machine Foundation Design: A Review Study. *E3S Web of Conferences*, 427. doi:10.1051/e3sconf/202342701029.
- [44] Noman, B. J., & Albusoda, B. S. (2024). Effect of Soil-Structure Interaction on the Response of Machine Foundation Subjected to Seismic Loading: A Review Study. *Journal of Engineering*, 30(04), 152–174. doi:10.31026/j.eng.2024.04.10.
- [45] Wood, D. M., Crewe, A., & Taylor, C. (2002). Shaking table testing of geotechnical models. *International Journal of Physical Modelling in Geotechnics*, 2(1), 01–13. doi:10.1680/ijpimg.2002.020101.
- [46] Lee, S. H., Choo, Y. W., & Kim, D. S. (2013). Performance of an equivalent shear beam (ESB) model container for dynamic geotechnical centrifuge tests. *Soil Dynamics and Earthquake Engineering*, 44, 102–114. doi:10.1016/j.soildyn.2012.09.008.
- [47] Alaie, R., & Jamshidi Chenari, R. (2018). Design and Performance of a Single Axis Shake Table and a Laminar Soil Container. *Civil Engineering Journal*, 4(6), 1326. doi:10.28991/cej-0309176.
- [48] Fiorino, L., Bucciero, B., & Landolfo, R. (2019). Evaluation of seismic dynamic behaviour of drywall partitions, façades and ceilings through shake table testing. *Engineering Structures*, 180, 103–123. doi:10.1016/j.engstruct.2018.11.028.
- [49] Fan, G., Zhang, J., Wu, J., & Yan, K. (2016). Dynamic Response and Dynamic Failure Mode of a Weak Intercalated Rock Slope Using a Shaking Table. *Rock Mechanics and Rock Engineering*, 49(8), 3243–3256. doi:10.1007/s00603-016-0971-7.
- [50] Hussein, A. F., & El Naggar, M. H. (2021). Seismic axial behaviour of pile groups in non-liquefiable and liquefiable soils. *Soil Dynamics and Earthquake Engineering*, 149, 106853. doi:10.1016/j.soildyn.2021.106853.
- [51] Xiao, C., Han, J., & Zhang, Z. (2016). Experimental study on performance of geosynthetic-reinforced soil model walls on rigid foundations subjected to static footing loading. *Geotextiles and Geomembranes*, 44(1), 81–94. doi:10.1016/j.geotexmem.2015.06.001.
- [52] Garala, T. K., & Madabhushi, G. S. P. (2021). Role of Pile Spacing on Dynamic Behavior of Pile Groups in Layered Soils. *Journal of Geotechnical and Geoenvironmental Engineering*, 147(3), 4021005. doi:10.1061/(asce)gt.1943-5606.0002483.
- [53] Robinsky, E. I., & Morrison, C. F. (1964). Sand Displacement and Compaction around Model Friction Piles. *Canadian Geotechnical Journal*, 1(2), 81–93. doi:10.1139/t64-002.
- [54] Cooke, R. W., & Price, G. (1973). Strains and displacements around friction pile. In: *Proc. 8th International Conference on Soil Mechanics and Foundation Engineering, Moscow*, 2, No.1, 53–60.
- [55] Puech, A. (1975). On the influence of compressibility on the limit bearing force of deep foundations. PhD Thesis, Université Grenoble Alpes, Saint-Martin-d'Hères, France. (In French).
- [56] Randolph, M. F., & Wroth, C. P. (1978). Analysis of Deformation of Vertically Loaded Piles. *Journal of the Geotechnical Engineering Division*, 104(12), 1465–1488. doi:10.1061/ajgeb6.0000729.
- [57] Dong, J., Chen, F., Zhou, M., & Zhou, X. (2018). Numerical analysis of the boundary effect in model tests for single pile under lateral load. *Bulletin of Engineering Geology and the Environment*, 77(3), 1057–1068. doi:10.1007/s10064-017-1182-5.
- [58] Alves, M., & Oshiro, R. E. (2006). Scaling impacted structures when the prototype and the model are made of different materials. *International Journal of Solids and Structures*, 43(9), 2744–2760. doi:10.1016/j.ijsolstr.2005.03.003.
- [59] Das, B. M., & Sivakugan, N. (2018). Principles of foundation engineering. Cengage Learning, Boston, United States.
- [60] ACI 351.3R. (2018). Report on foundations for Dynamic Equipment. American Concrete Institute (ACI), Michigan, United States.
- [61] Meymand, P. J. (1998). Shaking table scale model tests of nonlinear soil-pile-superstructure interaction in soft clay. Ph.D. Thesis, University of California, Berkeley, Berkeley, United States.
- [62] Wood, D. M. (2017). Geotechnical modelling. CRC press, Boca Raton, United States.
- [63] Das, B. M., & Luo, Z. (2016). Principles of soil dynamics. Cengage Learning, Boston, United States.
- [64] Thomson, W. T. (2018). Theory of Vibration with Applications. CRC Press, Boca Raton, United States. doi:10.1201/9780203718841.
- [65] Barkan, D. D., Drashevskaya, L., & Tschebotarioff, G. P. (1962). Dynamics of Bases and Foundations. McGraw-Hill Book Company, New York, United States.
- [66] Richart, F. E., Hall, J. R., & Woods, R. D. (1970). Vibrations of soils and foundations. Prentice Hall, Hoboken, United States.

- [67] Bommer, J. J., & Acevedo, A. B. (2004). The use of real earthquake accelerograms as input to dynamic analysis. *Journal of Earthquake Engineering*, 8(Sup001), 43–91. doi:10.1080/13632460409350521.
- [68] Krinitzky, E. L., & Chang, F. K. (1977). State-of-the-art for assessing earthquake hazards in the United States: Report 7, Specifying peak motions for design earthquakes. Waterways Experiment Station, Vicksburg, United States.
- [69] Meteoseism (2024). Iraqi Meteorological Organization and Seismology, Ministry of Transportation, Baghdad, Iraq. Available online: <http://meteoseism.gov.iq/> (accessed on September 2024). (In Arabic).
- [70] Al-Taie, A. J., & Albusoda, B. S. (2019). Earthquake hazard on Iraqi soil: Halabjah earthquake as a case study. *Geodesy and Geodynamics*, 10(3), 196–204. doi:10.1016/j.geog.2019.03.004.
- [71] CESMD (2024). El Centro 1940 Earthquake Strong Motion Data. Center for Engineering Strong-Motion Data (CESMD), Sacramento and Menlo Park, California, United States. Available online: <https://strongmotioncenter.org/> (accessed on September 2024).
- [72] USGS. (2024). Pazarcik earthquake, Kahramanmaras earthquake sequence. United States Geological Survey (USGS), Reston, United States. Available online: <https://earthquake.usgs.gov/earthquakes/eventpage/us6000jllz/executive> (accessed on September 2024).
- [73] CESMD (2024). Kobe 1995 Earthquake Strong Motion Data. Center for Engineering Strong-Motion Data (CESMD), Sacramento and Menlo Park, California, United States. Available online: <https://strongmotioncenter.org/> (accessed on September 2024).
- [74] Boudghene Stambouli, A., Zendagui, D., Bard, P. Y., & Derras, B. (2017). Deriving amplification factors from simple site parameters using generalized regression neural networks: Implications for relevant site proxies. *Earth, Planets and Space*, 69(1), 1–26. doi:10.1186/s40623-017-0686-3.
- [75] Meng, S. Bo, Zhao, J. Wei, Liu, Z. Xian, & Jin, W. (2022). Prediction and Modeling for Local Site Amplification Effect of Ground Motion: Exploring Optimized Machine Learning Approaches. *Pure and Applied Geophysics*, 179(5), 1805–1827. doi:10.1007/s00024-022-02997-y.
- [76] Zahoor, F., Satyam, N., & Rao, K. S. (2023). A Comprehensive Review of the Nonlinear Response of Soil Deposits and its Implications in Ground Response Analysis. *Indian Geotechnical Journal*, 54(3), 781–799. doi:10.1007/s40098-023-00798-1.
- [77] Hardin, B. O., & Drnevich, V. P. (1972). Shear Modulus and Damping in Soils: Measurement and Parameter Effects (Terzaghi Lecture). *Journal of the Soil Mechanics and Foundations Division*, 98(6), 603–624. doi:10.1061/jsfeaq.0001756.
- [78] Seed, H. B. (1970). Soil moduli and damping factors for dynamic response analyses. Report, EERC-70, National Technical Information Service, Springfield, United States
- [79] Kaynia, A. M. (1982). Dynamic stiffness and seismic response of pile groups. Ph.D. Thesis, Massachusetts Institute of technology, Cambridge, United States.
- [80] Manna, B., & Baidya, D. K. (2010). Dynamic nonlinear response of pile foundations under vertical vibration-Theory versus experiment. *Soil Dynamics and Earthquake Engineering*, 30(6), 456–469. doi:10.1016/j.soildyn.2010.01.002.
- [81] Rao, S. S. (2019). Mechanical vibrations, 1995. Addison-Wesley, Boston, United States.
- [82] Friswell, M. I. (2010). Dynamics of rotating machines. Cambridge university press, Cambridge, United Kingdom.
- [83] Thomson, W. (2018). Theory of vibration with applications. CRC Press, Boca Raton, United States.
- [84] Crouse, C. B., & Jennings, P. C. (1975). Soil-structure interaction during the San Fernando earthquake. *Bulletin of the Seismological Society of America*, 65(1), 13–36. doi:10.1785/bssa0650010013.
- [85] Wolf, J. P. (1994). Foundation vibration analysis using simple physical models. Pearson Education, London, United Kingdom.
- [86] Gazetas, G. (1984). Seismic response of end-bearing single piles. *International Journal of Soil Dynamics and Earthquake Engineering*, 3(2), 82–93. doi:10.1016/0261-7277(84)90003-2.
- [87] Crouse, C. B., & McGuire, J. (2001). Energy dissipation in soil-structure interaction. *Earthquake Spectra*, 17(2), 235–259. doi:10.1193/1.1586174.
- [88] Sugiyama, T., Maeda, K., & Kaneko, M. (1990). Traveling wave effects on a tall and narrow building: Observation and analysis. *Computers and Geotechnics*, 9(4), 307–324. doi:10.1016/0266-352X(90)90044-V.
- [89] Yamahara, H. (1970). Ground motions during earthquakes and the input loss of earthquake power to an excitation of buildings. *Soils and Foundations*, 10(2), 145–161. doi:10.3208/sandf1960.10.2_145.
- [90] Han, Y. C., & W. Sabin, G. C. (1995). Impedances for Radially Inhomogeneous Viscoelastic Soil Media. *Journal of Engineering Mechanics*, 121(9), 939–947. doi:10.1061/(asce)0733-9399(1995)121:9(939).

- [91] Sugiyama, T., Ishii, T., & Kaneko, M. (1995). Effects of seismic wave propagation on a long and narrow building: Body wave and surface wave propagation. *Computers and Geotechnics*, 17(4), 547–564. doi:10.1016/0266-352X(95)94919-H.
- [92] Day, R. W. (2002). *Geotechnical Earthquake Engineering*. The Civil Engineering Handbook, CRC Press, Boca Raton, United States.
- [93] Chopra, A. K. (2007). *Dynamics of structures*. Pearson Education India, Delhi, India.
- [94] Prasad, B. B. (2009). *Fundamentals of soil dynamics and earthquake engineering*. PHI Learning Private Limited, New Delhi, India.
- [95] Sarrazin, M. A., Roesset, J. M., & Whitman, R. V. (1972). Dynamic Soil-Structure Interaction. *Journal of the Structural Division*, 98(7), 1525–1544. doi:10.1061/jsdeag.0003278.
- [96] Yeh, C. H., & Wen, Y. K. (1990). Modeling of nonstationary ground motion and analysis of inelastic structural response. *Structural Safety*, 8(1–4), 281–298. doi:10.1016/0167-4730(90)90046-R.
- [97] Cao, H., Yang, H., Friswell, M. I., & Bai, S. (2004). The Analysis of Earthquake Waves Based on Nonlinear Responses of RC Structures. *ESDA2004-58253*, 69–74. doi:10.1115/esda2004-58253.
- [98] Qu, G., Liu, X., & Yu, R. (2017). Practical Simulation Method of Non-Stationary Earthquake Ground Motion Based on Frequency-Dependent Amplitude Envelope Function. *International Collaboration in Lifeline Earthquake Engineering 2016*, 23, 405–411. doi:10.1061/9780784480342.055.
- [99] Veletsos, A. S., & Meek, J. W. (1974). Dynamic behaviour of building-foundation systems. *Earthquake Engineering & Structural Dynamics*, 3(2), 121–138. doi:10.1002/eqe.4290030203.
- [100] Mylonakis, G., & Gazetas, G. (2000). Seismic soil-structure interaction: Beneficial or detrimental? *Journal of Earthquake Engineering*, 4(3), 277–301. doi:10.1080/13632460009350372.
- [101] Beresnev, I. A., & Wen, K.-L. (1996). Nonlinear soil response—A reality? *Bulletin of the Seismological Society of America*, 86(6), 1964–1978. doi:10.1785/bssa0860061964.
- [102] Kramer, S. L. (1996). *Geotechnical earthquake engineering*. Prentice Hall, Hoboken, United States.
- [103] Inman, D. J. (1989). *Vibration: with control, measurement, and stability*. Prentice Hall, Hoboken, United States.
- [104] Ehrich, F.F. (1992) *Handbook of Rotordynamics*. McGraw-Hill, New York, United States.
- [105] Gutierrez-Wing, E. S. (2003). *Modal analysis of rotating machinery structures*, Ph.D. Thesis, University of London, London, United Kingdom.
- [106] Zheng, X., Jin, Y., Cai, R., Rabczuk, T., Zhu, H., & Zhuang, X. (2024). Elastic surface wave attenuation in layered soil by metastructures. *Low-Carbon Materials and Green Construction*, 2(1), 5. doi:10.1007/s44242-024-00037-7.